

The synthesis and structural requirements for measuring glucocorticoid receptor expression in vivo with (\pm)- ^{11}C -YJH08 PET

Yangjie Huang¹, Ning Zhao¹, Yung-hua Wang¹, Charles Truillet², Junnian Wei¹, Matthew F.L. Parker¹, Joseph E. Blecha¹, Christopher R. Drake³, Henry F. VanBrocklin^{1,4}, Diego Garrido-Ruiz⁵, Matthew P. Jacobson⁵, Rahul Aggarwal^{4,6}, Spencer C. Behr¹, Robert R. Flavell^{1,4}, David M. Wilson¹, Youngho Seo^{1,4}, Michael J. Evans^{1,4,5}

¹Department of Radiology and Biomedical Imaging, University of California, San Francisco, San Francisco, CA 94158.

²Imagerie Moleculaire in Vivo, INSERM, CEA, Université Paris Sud, CNRS, Université Paris Saclay, CEA-Service Hospitalier Frederic Joliot, Orsay 94100, France

³Sofie Biosciences, 6160 Bristol Pkwy Suite 200, Culver City, CA 90230

⁴Helen Diller Family Comprehensive Cancer Center, University of California, San Francisco, San Francisco, CA 94158.

⁵Department of Pharmaceutical Chemistry, University of California, San Francisco, San Francisco, CA 94158.

⁶Department of Medicine, Division of Hematology/Oncology, University of California San Francisco, San Francisco, CA 94158

Corresponding author:

Name: Michael J. Evans, PhD

Address: 600 16th Street, N572C

University of California San Francisco, San Francisco, CA 94158

Telephone/Fax: (415) 514-1292/(415) 353-9425

E-mail: michael.evans@ucsf.edu

First author:

Name: Yangjie Huang, PhD.

Address: 600 16th Street, N552

University of California San Francisco, San Francisco, CA 94158

Telephone number: (415) 769-9292

E-mail: yangjie.huang@ucsf.edu

Short title: (\pm)-¹¹C-YJH08 PET to measure GR expression

Financial Support: This study was supported by National Institute of Mental Health (R01MH115043) and the Prostate Cancer Research Program of the Congressionally Directed Medical Research Programs (W81XWH-15-1-0552).

Word count: 4,772

ABSTRACT

Non-invasive methods to study glucocorticoid receptor (GR) signaling are urgently needed to elaborate the complexity of GR signaling in normal physiology and human disorders, as well as to identify selective GR modulators to treat diseases. Here, we report evidence supporting translational studies with (\pm)- ^{11}C -5-(4-fluorobenzyl)-10-methoxy-2,2,4-trimethyl-2,5-dihydro-1H-chromeno[3,4-f]-quinoline (named as (\pm)- ^{11}C -YJH08), a radioligand for positron emission tomography (PET) that engages the ligand binding domain on GR. **Methods:** (\pm)- ^{11}C -YJH08 was synthesized by reacting the phenol precursor with ^{11}C -methyl iodide. The biodistribution was studied in vivo. Specific binding was tested in vivo with adrenalectomy and ligand competition. A library of analogues was synthesized and studied in vitro and in vivo to understand the (\pm)- ^{11}C -YJH08 structure activity relationship. Rodent dosimetry studies were performed to estimate the human equivalent doses of (\pm)- ^{11}C -YJH08. **Results:** (\pm)- ^{11}C -YJH08 was synthesized by reaction of the phenolic precursor with ^{11}C -methyl iodide giving a radiochemical yield of $51.7 \pm 4.7\%$ (decay corrected to starting ^{11}C -methyl iodide). Specific binding was observed in many tissues, including the brain. An analysis of the (\pm)-YJH08 structure-activity relationship showed that (*R*)- and (*S*)-enantiomers are equally avid for GR by occupying discrete binding modes. A focused chemical screen revealed that the aryl fluoride motif on YJH08 is essential for high affinity GR binding in vitro, high tissue uptake in vivo, and efficient passage across the blood brain barrier. Lastly, we performed dosimetry studies in rodents, from which we estimated human equivalent doses of (\pm)- ^{11}C -YJH08 to be commensurate with widely used carbon-11 and fluorine-18 tracers. **Conclusion:** In summary, these studies reveal the molecular determinants of a high affinity and selectivity ligand-receptor interaction and support the use of (\pm)- ^{11}C -YJH08 PET to make the first measurements of GR expression in human subjects.

Keywords: glucocorticoid receptor (GR), carbon-11, molecular imaging, dosimetry study, positron emission tomography

INTRODUCTION

The glucocorticoid receptor (GR) is a nuclear hormone receptor whose expression and activity (genomic and non-genomic) regulates a remarkable breadth of cellular processes (1). Moreover, dysregulation of GR signaling is known or suspected to drive the pathobiology of numerous human diseases, including endocrine disorders, pulmonary diseases, mood disorders, and even cancers (2-3). That said, fully articulating the role of GR in human biology has been challenging because the scientific community lacks safe and efficacious technologies to measure GR expression and/or activity in living human subjects. Moreover, while therapeutic modulators of GR are in routine clinical use (e.g. dexamethasone, mifepristone), their limitations are well characterized and due in part to on-target, off-tissue drug interactions (4). Thus, non-invasive biomarkers to study GR signaling could enable drug discovery efforts to identify more specific GR modulators.

Appreciating these unmet needs, the nuclear medicine community has attempted for over three decades to develop radiolabeled probes to measure GR expression in vivo with quantitative imaging modalities (5). Previous radioligands bore at least one of the following shortcomings: a low yielding radiosynthesis, poor in vivo stability, or limited evidence of specific receptor binding in vivo. We recently developed (\pm)-¹⁸F-YJH08, a promising non-steroidal radioligand built on a benzopyrano[3,4-f]quinoline scaffold that appears to overcome these challenges (6). In vitro, the ligand is a potent and specific GR binder with milder agonism compared to dexamethasone. In vivo, the tracer specifically bound to GR in many normal mouse tissues of relevance to corticosteroid endocrinology (e.g. the adrenals) and achieved the highest level of specific brain uptake reported to date. Moreover, (\pm)-¹⁸F-YJH08 PET revealed an entirely unexpected tissue selective pharmacological interaction between GR and an HSP70 inhibitor. These data inspired us to carry out the current study, which was aimed at refining the structure and chemistry of the radioligand with an eye toward translation.

Herein, we provide evidence advocating for the clinical translation of (\pm)-¹¹C-YJH08. For example, radiolabeling the phenol precursor of (\pm)-YJH08 using ¹¹C-methyl iodide resulted in higher radiochemical yield and specific activity compared to (\pm)-¹⁸F-YJH08. The in vivo stability of (\pm)-¹¹C-YJH08 was also measured to be >90%. Studying the YJH08 structure activity relationship showed that (*R*) and (*S*) enantiomers had similar biodistribution profiles in vivo, which was consistent with in vitro affinity data and molecular dynamics simulations predicting approximately equal affinities for GR. A focused chemical screen revealed that the aryl fluoride

group on the C5 position of the benzopyrano[3,4-f]quinoline scaffold was essential for high affinity binding to GR. Moreover, a biodistribution study with ^{11}C -2,5-dihydro-10-methoxy-5-oxo-2,2,4-trimethyl-1H-[1]benzopyrano [3,4-f]quinoline (termed ^{11}C -YJH02) showed that the aryl fluoride motif is critical to tissue uptake and blood brain barrier penetrance. Lastly, we performed a rodent dosimetry study with (\pm)- ^{11}C -YJH08 which showed that the human equivalent effective dose is equal or less than other carbon-11 or fluorine-18 small molecule radiotracers in widespread clinical use, for example ^{11}C -Pittsburgh Blue and ^{18}F -Fluorodeoxyglucose (7-9). Collectively, these data support the translation of (\pm)- ^{11}C -YJH08 for human imaging trials to study GR expression in normal subjects and patients, and to parse the pharmacology of GR modulators.

METHODS

All synthetic details and additional experimental methods are provided in Supporting Information. In vitro affinity assays were performed as previously reported in reference #6.

Radiosynthesis of (\pm)- ^{11}C -YJH08, *R*- ^{11}C -YJH08 and *S*- ^{11}C -YJH08

^{11}C -CO₂ was produced in target by the $^{14}\text{N}(\text{p},\text{a})^{11}\text{C}$ nuclear reaction of 17 MeV protons on N₂ at the University of California San Francisco (UCSF) Radiopharmaceutical facility. ^{11}C -CO₂ was converted to ^{11}C -MeI using the gas-phase method on a GE FX/C Pro automated synthesis module. In a 3 mL V-type vial, the phenol **7** (1 mg, 2.5 μmol) was pre-mixed with DMF (0.6 mL), 1.1 equiv of KOH (aq) and 20 equiv of K₂CO₃ (aq), and then stirred at room temperature for 10 min. ^{11}C -MeI (g) was transferred into the reaction vial at room temperature. The reaction mixture was stirred for another 10 min at 85 °C and neutralized with HCl (aq). The reaction mixture was subjected to the semipreparative HPLC for the purification, which took 10 min and provided the radioactive product in a decay-corrected radiochemical yield of 51.7 ± 4.7 % (n = 8). The semipreparative HPLC condition was as follows: Waters C18 (19 mm \times 50 mm, 5 μm), mobile phase acetonitrile/H₂O (30% to 95% CH₃CN in water over 12 min, then 95% CH₃CN for 8 min); flow rate = 10 mL/min.

To prepare the radiotracer for animal studies, (\pm)- ^{11}C -YJH08 was trapped on the cartridge and eluted with CH₃CN (1 mL). After removing the organic solvent, the pure product was dissolved in an injection formulation of 1/1/8 (v/v/v) DMSO/Tween 80/Saline. The stability, UV

purity, and radiochemical purity of (\pm)- ^{11}C -YJH08 in formulation was further confirmed by analytical HPLC equipped with a gamma ray radio detector and a UV detector at 254 nm. The analytical HPLC condition was as follows: Waters C18 (4.6 mm \times 150 mm, 5 μm), mobile phase acetonitrile/ H_2O , 8:2 (v/v); flow rate = 1 mL/min. Both the UV and Rad spectrum comigrated with the analytical standard, and the purity of the tracer was >95%.

R - ^{11}C -YJH08 and S - ^{11}C -YJH08 were synthesized using the same procedure as above from corresponding enantiopure phenol precursor.

Animal Studies

All animal experiments were performed under the approval of the Institutional Animal Care and Use Committee (IACUC) at UCSF. C57BL6/J mice (4–6 weeks) were purchased from Charles River. All the mice were housed in a dedicated vivarium with free access to food and water. For dexamethasone treatment studies, dex was administered via two routes involving oral gavage of 50 mg/kg (formulation: 0.5% hydroxy-propyl-methylcellulose and 0.2% Tween 80 in water) for three days prior to radiotracer injection or administration of a water soluble dexamethasone-cyclodextrin (CD) complex via intraperitoneal injection at 10 mg/kg in PBS one hour prior to radiotracer injection. Adrenalectomized mice were purchased from Charles River and provided drinking water supplemented with NaCl (aq) per instructions until the time of the tracer biodistribution study.

Serum Stability Studies

Mice were euthanized, received radiotracer (30 MBq in 100-150 μL formulation) via tail injection, and dissected at dedicated time points post injection. The blood was collected and an aliquot (50 μL) was mixed with CH_3CN (50 μL). The serum proteins were precipitated out and followed by a centrifugation (10000 rpm for 5 min). The cleared supernatant (50 μL) was collected and further analyzed by RAD-iTLC.

Plasma Protein Binding Studies

The rapid equilibrium dialysis (RED) device inserts along with a Teflon base plate (Pierce, Rockford, IL) were used for the binding studies. The pH of the human or mouse plasma was adjusted to 7.4 prior to the experiment. DMSO stocks (1 mM) were spiked into the plasma to make a final

concentration of 2 μM . The spiked plasma solutions (300 μL) were placed into the sample chamber (indicated by the red ring); and 500 μL of PBS buffer, pH 7.4, was placed into the adjacent chamber. The plate was incubated at 37°C on an orbital shaker (250 rpm) for 4 hours.

After 4 hours, from the RED plate, aliquots (100 μL) were removed from each side of the insert (plasma and buffer) and dispensed into the 96-well plate. Subsequently, 100 μL of blank plasma was added to the buffer samples and 100 μL of blank buffer was added to all the collected plasma samples. 300 μL of quench solution (50% acetonitrile, 50% methanol, and 0.05% formic acid, warmed up at 37°C) containing internal standards was added to each well. Plates were sealed, vortexed, and centrifuged at 4°C for 15 minutes at 4000 rpm. The supernatant was transferred to fresh plates for LC/MS/MS analysis. The sample were analyzed on LC/MS/MS using an AB Sciex API 4000 instrument, coupled to a Shimadzu LC-20AD LC Pump system. Analytical samples were separated using a Waters Atlantis T3 dC18 reverse phase HPLC column (20 mm x 2.1 mm) at a flow rate of 0.5 mL/min. The mobile phase consisted of 0.1% formic acid in water (solvent A) and 0.1% formic acid in acetonitrile (solvent B).

The percentage of test compound bound to protein was calculated by the following equation:

$$\% \text{ Free} = (\text{Concentration in buffer chamber} / \text{Concentration in plasma chamber}) \times 100\%$$

$$\% \text{ Bound} = 100\% - \% \text{ Free}$$

Small animal PET/CT Imaging

Data were acquired with a Siemens Inveon microPET/CT. For dynamic acquisitions, the mice were anesthetized prior with 1.5 – 2% isoflurane and positioned on the scanner bed, then approximately 30 MBq of (\pm)- ^{11}C -YJH08 was injected via tail vein in a volume of 100–150 μL per mouse. All PET imaging data were decay corrected, reconstructed with CT-based attenuation correction, and analyzed with AMIDE software. Regions of interest were manually placed to calculate SUV mean data from the dynamic acquisitions.

Biodistribution Studies

Mice were euthanized after radiotracer (7.4 – 18.5 MBq in 100-150 μL) injection with CO_2 (g) asphyxiation and dissected at dedicated time points post injection. The blood and tissues were collected, washed, dried, and weighed. The activity of each tissue was measured with a gamma counter. All data was decay corrected. PRISM software was used to express a percentage (% ID/g) of the injected dose per gram of tissue.

Normal Tissue Radiation Dose Estimation

Volumes of interest (VOIs) were drawn on coregistered CT images for brain, lungs, heart, liver, stomach, kidneys, and urinary bladder. All VOIs were either elliptical cylinder (5 mm long axis, 3 mm short axis, and 5 mm height for the brain), cylinders (3 mm diameter and 3 mm height for kidneys), or spheres (3 mm diameter for lungs, heart, liver, stomach, and urinary bladder), and they were placed well within the anatomical boundaries to minimize spill-over or spill-in of radioactivity. The mean values (in Bq/ml) in these VOIs were multiplied by standard mouse organ volumes (in ml) to estimate total activity (in Bq) within these organs. The total activity within the entire animal subtracted by all organ activities was used as activity in the remainder of the body. The percent of injected activity within the defined organs (%IA) was extrapolated to human-equivalent values using ratios of standard human organ weights to mouse organ weights.

These input %IA data for each organ and the remainder of the body were curve-fitted to derive time-integrated activity coefficients (also known as residence times) (in Bq-hr/Bq) and organ and whole-body effective doses for human equivalents were estimated using each mouse data. The data from the three animals were averaged to derive absorbed organs doses (in mGy/MBq) and whole-body effective dose (in mSv/MBq). Organ and effective dose estimations were performed using OLINDA version 2.0 using ICRP Publication 103 tissue weighting factors.

Autoradiography

After 20 min post-injection of (\pm)- ^{11}C -YJH08 (~ 30 MBq per mouse), mice were anesthetized and were perfused with cold PBS via cardiac puncture. Tissues were immediately collected, and flash frozen in OCT on dry ice. Tissues were sectioned on a microtome at a thickness of 20 μm and immediately mounted on glass slides. The slides were then exposed on a GE phosphor storage screen, and the screen was developed on an Amersham Typhoon 9400 phosphorimager. The autoradiography images were processed using ImageJ software.

Statistics

All statistical analysis was performed using PRISM v8.0 software. An unpaired, two-tailed Student's t test was used to determine statistically significant differences in the data. $P < 0.05$ was

reported as statistically significant. For the determination of K_i , the data were fit with a one site nonlinear regression model.

Radiochemical Synthesis of ^{11}C -YJH02

^{11}C -MeI (g) was transferred from a Porapak N column into a glass reactor vial cooled in an ice/water bath containing 1 mg precursor and 5 mg Cs_2CO_3 dissolved in 600 μL DMF. After transfer was complete, the vial was stirred at r.t. for 10 minutes, after reaction completed and diluted with water. The solution was loaded on reverse-phase semi-preparatory HPLC. The product containing fraction was diluted with 30 mL water and loaded onto a C18-light Sep-Pak cartridge. The Sep-Pak was washed with water and the product was eluted with 300 μL ethanol. The solution was diluted with buffered saline and use in subsequent experiments. The tracer was obtained in $70 \pm 8\%$ ($n = 4$) decay-corrected yield with greater than 95% purity. HPLC condition was as follows: Waters C18 (19 mm \times 50 mm, 5 μm), mobile phase acetonitrile/ H_2O : 6:4 (v/v); flow rate = 10 mL/min. The stability, UV purity, and radiochemical purity of ^{11}C -YJH02 in formulation was further confirmed by analytical HPLC equipped with a gamma ray radio detector and a UV detector at 254 nm. The analytical HPLC condition was as follows: Waters C18 (4.6 mm \times 150 mm, 5 μm), mobile phase acetonitrile/ H_2O , 6:4 (v/v); flow rate = 1 mL/min. Both the UV and Rad spectrum comigrated with the analytical standard, and the purity of the tracer was >95%

RESULTS

Radiochemical Synthesis of (\pm)- ^{11}C -YJH08.

The synthesis of the phenol **7** was achieved following the approach outlined in Supplemental Fig. 1. The hydroxy group on the C10 position was chosen as the site for modification with carbon-11 owing to well established chemical precedents for alkylating phenols with electrophiles like ^{11}C -methyl iodide or ^{11}C -methyl triflate (**10**). To synthesize the precursor, the phenol on compound **2** was protected as a tert-butyldimethyl silyl ether. After adding the 4-fluorobenzyl motif via Grignard chemistry, the silyl ether was removed to afford the phenol **7**. Prior to conducting the radiochemistry, a model cold alkylation was performed on **7** with methyl iodide. The reaction proceeded smoothly and conferred **8** to high yield.

The radiosynthesis of (\pm)- ^{11}C -YJH08 is shown in Figure 1A. After some optimization (Supplemental Table 1), the highest yielding conditions were achieved by pre-mixing 7 with DMF (0.6 mL), 1.1 equiv of KOH (aq) and 20 equiv of K_2CO_3 (aq) in the 3 mL vial, and then stirring at room temperature for 10 min. ^{11}C -methyl iodide (prepared from ^{11}C - CO_2 , see also Supplemental Materials) was transferred into the reaction vial at room temperature. The reaction mixture was stirred for another 10 min at 85°C and neutralized with HCl (aq). The mixture was purified using semipreparative HPLC with a C-18 column (Figure 1B). The final decay corrected radiochemical yield from 14,800 MBq of ^{11}C -MeI was approximately $2,590 \pm 103.6$ MBq, or $50 \pm 4\%$ ($n = 6$). The radiochemical purity, which was evaluated by reinjecting purified radiotracer over two HPLC conditions (Supplemental Fig. 2), was consistently greater than 95%, and the molar activity was 37 ± 7.4 GBq/ μmol (Supplemental Fig. 3).

In vivo Imaging Studies with (\pm)- ^{11}C -YJH08.

We next conducted a dynamic PET acquisition in C57BL6/J mice to determine the radiotracer biodistribution in vivo. Region of interest analysis of the 60 min scan showed that (\pm)- ^{11}C -YJH08 rapidly cleared from the serum and the primary mode of clearance appeared to be hepatobiliary (Figure 1C). Moreover, tracer uptake in several organs of interest to GR biology (e.g. kidneys, brain, and adipose tissue) were above the reference compartments of blood and muscle levels at 90 min post injection and saturable over time (Figure 1C). To confirm stability, we collected blood at 30 minutes post injection, a time point after which we previously showed specific binding in vivo with (\pm)- ^{18}F -YJH08. Resolution of the radiolabeled metabolites on ITLC suggested the radiotracer was $>90\%$ stable at this time point (Supplemental Fig. 4). We also conducted a plasma protein binding assay to determine the percentage of free versus protein bound compound. (\pm)-YJH08 was almost completely bound to mouse or human serum protein (Supplemental Table 2), which suggests that the ligand, like endogenous corticosteroids, utilizes corticosteroid binding globulin to traffic to tissues (11). Lastly, comparing the tissue uptake of carbon-11 versus fluorine-18 labeled (\pm)-YJH08 in C57Bl6/J mice at 20 min post injection showed no significant differences (Table 1).

We then probed for evidence of specific binding by (\pm)- ^{11}C -YJH08 in vivo. We first treated wild type C57Bl6/J mice with dexamethasone for three days via oral gavage (50 mg/kg), an approach that we previously used to saturate GR in vivo (6, 12). Dexamethasone treatment by this

route significantly reduced (\pm)- ^{11}C -YJH08 uptake in numerous normal tissues (Figure 2A and Supplemental Table 3). We also evaluated whether acute dosing with a more bioavailable formulation of dexamethasone in complex with cyclodextrin (Dex-CD) suppresses (\pm)- ^{11}C -YJH08 binding in tissues. Significant reductions in (\pm)- ^{11}C -YJH08 tissue uptake were observed by treating mice with Dex-CD at 10 mg/kg via intraperitoneal injection 1 hour before the radiotracer injection (Figure 2A). Notably, both blocking approaches significantly reduced tracer binding in the brain (Figure 2A). Comparing the relative suppression of radiotracer binding across tissues showed that chronic, high doses of dexamethasone generally resulted in more significant blockade of radiotracer binding per tissue, consistent with a GR specific dose response (Figure 2B). Visually inspecting the decay corrected PET data showed (\pm)- ^{11}C -YJH08 suppression by dexamethasone in several tissue compartments, for example, the brain, the supraspinal depot of brown fat, and the liver (Figure 2C). We further studied specific binding in vivo by investigating relative tissue uptake in intact versus adrenalectomized mice (adrenalectomy depletes serum corticosteroids and elevates GR expression in tissues). As expected, tracer uptake was significantly higher in several tissues of adrenalectomized mice, including the brain (Supplemental Table 4). Moreover, the relative induction of radiotracer uptake per tissue in adrenalectomized versus intact mice was qualitatively very similar between (\pm)- ^{11}C - and ^{18}F -YJH08 (Supplemental Fig. 5A). Lastly, we compared the radiotracer uptake within the brain using autoradiography and observed that the overall patterns of (\pm)- ^{11}C - and ^{18}F -YJH08 binding were qualitatively similar between representative brain sections equidistant from bregma (Supplemental Fig. 5B).

Enantiomers of YJH08 are equipotent for GR and have similar biodistribution profiles in vivo

Since YJH08 is a racemic mixture, we next tested whether the (*R*) and (*S*) enantiomers behaved differently in vitro and in vivo, which could provide a rationale for translating enantiomerically pure YJH08. The racemic mixture of the phenol **7** was resolved using a chiral Lux[®] 5 μ Cellulose-1 stationary phase with an isocratic mobile phase of 30% water, 70% acetonitrile, and 0.1% trifluoroacetic acid (*v/v*) (Figure 3A). We isolated several mgs of one peak and recrystallized the compound in hexanes. X ray crystallography showed the peak eluting at 29.1 min to be the (*R*) enantiomer (Figure 3B and Supplemental Table 5). We next tested the in vitro affinity of each enantiomer for GR on cells using a ^3H -dexamethasone displacement assay.

(*R*) and (*S*) enantiomers had equivalent low nM affinity for GR, with K_i values of 3.76 nM (95% confidence interval = 2.93 – 4.8) and 2.03 nM (95% confidence interval = 0.78 – 5.3), respectively (Figure 3C). Thus, the enantiomers are equipotent with dexamethasone and have approximately 2 fold higher affinity than endogenous corticosteroids like cortisol or corticosterone.

The (*R*) and (*S*) phenol were then radiolabeled with ^{11}C -methyl iodide using the protocol outlined above. Each enantiomer labeled effectively to 55% and 48% respective decay corrected radiochemical yield from starting ^{11}C -methyl iodide (Supplemental Fig. 6). A biodistribution study in C57Bl6/J mice showed that tissue uptake of both enantiomers was very similar to each other (and racemic ^{11}C -YJH08) at 20 min post injection (Figure 3D).

These somewhat surprising results prompted us to probe the structural basis of the YJH08/GR interaction with molecular dynamics simulations. For docking studies, we used as a scaffold a co-crystal structure of the GR ligand binding domain with the corticosteroid agonist budesonide (PDB: 5NFP). Both enantiomers of YJH08 (Figure 3E) were prepared using the ligand preparation protocol in Maestro® and then docked into the binding site. We ran single precision (SP) and extra precision (XP) docking calculations with a flexible ligand and rigid receptor, within Maestro®'s docking suite. The resulting scores, SP: -7.3 (*S*), -8.1(*R*); XP: -7.3 (*S*), -8.1(*R*), were similar in value. Upon analysis of the binding pose within the site, we observed hydrophobic interactions (Figure 3E). Collectively, these data show that the ligand binding domain on GR can accommodate both enantiomers through hydrophobic interactions.

Analysis of the Structure Activity Relationship for YJH08 Reveals the Importance of an Aryl Moiety on the C5 Position to Affinity for GR and Uptake into the Brain.

To better understand the structure activity relationship between YJH08 and GR, we performed a focused chemical screen of five YJH08 analogues bearing diverse moieties on the C5 position of the scaffold (Supplemental Methods). The in vitro affinities of YJH01-5 for GR were determined and show that an aromatic group extending from the C5 position is important for a high affinity binding (Table 2 and Supplemental Fig. 7).

To understand the impact of the C5 moiety on in vivo biodistribution, we radiolabeled the phenolic precursor to YJH02 (which bears a carbonyl at the C5 position) via alkylation with ^{11}C -methyl iodide (Figure 4A and Supplemental Fig. 8). The final decay corrected radiochemical yield

from 18,500 MBq of ^{11}C -MeI was approximately $4,670 \pm 534$ MBq, or $70 \pm 8\%$ ($n = 4$). The radiochemistry purity was greater than 95%. A biodistribution study was conducted 20 min post injection in mice to determine specific binding in tissues (Figure 4B and Supplemental Table 6). Tracer uptake was suppressed in several tissues from mice treated intraperitoneally with Dex-CD compared to those treated with vehicle. Moreover, the overall pattern of tracer uptake was qualitatively similar to what was observed with $(\pm)\text{-}^{11}\text{C}$ -YJH08, with the highest uptake observed in the liver, large and small intestine, kidney, and heart. Directly comparing the uptake values in %ID/g of ^{11}C -YJH02 versus $(\pm)\text{-}^{11}\text{C}$ -YJH08 showed that ^{11}C -YJH02 levels were generally lower (Figure 4C). A stark difference in brain uptake was noted, and ^{11}C -YJH02 uptake was approximately three fold lower than what was observed for $(\pm)\text{-}^{11}\text{C}$ -YJH08 (Figure 4C). These data point to the importance of the benzyl fluoride group for high affinity interactions with GR and access to GR within tissues of high importance to GR (patho)biology.

A Rodent Dosimetry Study shows that Human Equivalent Organ Doses for $(\pm)\text{-}^{11}\text{C}$ -YJH08 align with other Carbon-11 and Fluorine-18 Radiotracers currently in Human use.

To explore the potential of $(\pm)\text{-}^{11}\text{C}$ -YJH08 for human translation, we conducted a rodent dosimetry study in male and female C57Bl6/J mice ($n = 4/\text{gender}$). The human equivalent doses for an average adult male (73 kg) or an average adult female (60 kg) were calculated using OLINDA 2.0 incorporating ICRP103 tissue weighting factors based on region of interest analysis from 90 min dynamic PET acquisitions (Table 3). The organs with the highest absorbed doses were the heart, stomach wall, liver, and thymus. All these tissues abundantly express GR, and in the case of the liver, the hepatobiliary mode of clearance (a slower process than renal clearance) for $(\pm)\text{-}^{11}\text{C}$ -YJH08 may contribute to the absorbed dose. The estimated whole-body effective dose to an adult male was 0.0067 ± 0.002 mSv/MBq and 0.0065 ± 0.004 mSv/MBq to an adult female. These values are comparable to those of other carbon-11 radiotracers that have been studied in humans, for example ^{11}C -Pittsburgh Compound B, and smaller than a calculated effective dose for ^{18}F -fluorodeoxyglucose (7-9).

DISCUSSION AND CONCLUSIONS

Here, we report data supporting the clinical translation of (\pm)- ^{11}C -YJH08 to study GR biology in humans. The radiosynthesis of (\pm)- ^{11}C -YJH08 was higher yielding than what we previously reported for (\pm)- ^{18}F -YJH08, and biodistribution studies showed equivalence to (\pm)- ^{18}F -YJH08. Importantly, the average final production yield of 2590 ± 103.6 MBq is sufficient for subsequent clinical translation. Somewhat unexpectedly, both the (*R*) and (*S*) enantiomers of YJH08 were predicted to have equal affinities for GR, and their *in vivo* patterns of biodistribution were mutually indistinguishable. Corticosteroid withholding and supplementation studies revealed evidence of specific binding for (\pm)- ^{11}C -YJH08 *in vivo*. Radioligand suppression was not achieved to equivalent extents in all tissues, although this could reflect our inability to safely saturate GR *in vivo*. Notably, we did previously observe dramatic suppression of (\pm)- ^{18}F -YJH08 uptake in the adipose tissue of an adipocyte specific GR knockout mouse, which adds support to a model for GR specific binding *in vivo* for this ligand structure.

Analysis of the YJH08 structure activity relationship *in vitro* established the importance of the benzyl moiety on the C5 position to GR affinity. Moreover, a biodistribution study with ^{11}C -YJH02 showed the importance of the benzyl fluoride group to tissue uptake *in vivo*, especially in compartments like the brain that can be challenging to access. The altered biodistribution of ^{11}C -YJH02 may be attributable to somewhat lower affinity for GR (Table 2). In addition, lower blood pool activity was observed for ^{11}C -YJH02 at 20 min post injection, which could indicate that lower tissue uptake is due to altered pharmacokinetics. Further studies are required to parse these mechanisms more systematically. Finally, a dosimetry study estimated the human equivalent doses of (\pm)- ^{11}C -YJH08 to be within the range of carbon-11 and fluorine-18 radiotracers that are in human use. Collectively, these data support the feasibility of human imaging studies with (\pm)- ^{11}C -YJH08 to study GR biology. Moreover, with experimental GR modulators entering clinical trials (e.g. ORIC-101), (\pm)- ^{11}C -YJH08 could be a useful companion diagnostic to identify tissues with altered GR expression and assess drug pharmacodynamics as has been previously done with radioligands targeting the androgen receptor and the estrogen receptor (13-15).

ACKNOWLEDGEMENTS

We gratefully acknowledge M. James and A. Chaney of Stanford University for assistance with digital autoradiography and T. Huynh for technical assistance with small animal PET/CT studies. M. J. Evans acknowledges funding from the National Institute of Mental Health (R01MH115043) and the Prostate Cancer Research Program of the Congressionally Directed Medical Research Programs (W81XWH-15-1-0552).

DECLARATIONS

The authors do not have any competing interests.

KEY POINTS

QUESTION: Studying GR expression in normal human physiology and disease is an outstanding challenge for the field due to the lack of non-invasive biomarkers.

PERTINENT FINDINGS: We synthesized ^{11}C -5-(4-fluorobenzyl)-10-methoxy-2,2,4-trimethyl-2,5-dihydro-1H-chromeno[3,4-f]quinoline (^{11}C -YJH08) a radioligand that potently and specifically binds GR. We further defined the structural determinants for the high affinity GR-ligand interaction, as well as the features of the molecule that promote specific binding in vivo. Lastly, we calculated the human dosimetry estimates.

IMPLICATIONS FOR PATIENT CARE: These studies support the use of (\pm)- ^{11}C -YJH08 PET to make the first measurements of GR expression in human subjects, which will further deepen our understanding of GR's role in human physiology or disease and aid in the development of selective GR modulators.

REFERENCES

1. De Kloet ER, Vreugdenhil E, Oitzl MS, Joels M. Brain corticosteroid receptor balance in health and disease. *Endocr Rev*. 1998;19:269-301.
2. Oakley RH, Cidlowski JA. The biology of the glucocorticoid receptor: new signaling mechanisms in health and disease. *J Allergy Clin Immunol*. 2013;132:1033-44.
3. Conzen SD. Recent advances in understanding glucocorticoid receptor function in cancer. *Clin Adv Hematol Oncol*. 2017;15:338-340.
4. Sundahl N, Bridelance J, Libert C, De Bosscher K, Beck IM. Selective glucocorticoid receptor modulation: New directions with non-steroidal scaffolds. *Pharmacol Ther*. 2015;152:28-41.
5. Steiniger B, Kniess T, Bergmann R, Pietzsch J, Wuest FR. Radiolabeled glucocorticoids as molecular probes for imaging brain glucocorticoid receptors by means of positron emission tomography (PET). *Mini Rev Med Chem*. 2008;8:728-39.
6. Huang Y, Zhao N, Wang YH, et al. A novel radioligand reveals tissue specific pharmacological modulation of glucocorticoid receptor expression with positron emission tomography. *ACS Chem Biol*. 2020;15:1381-1391.
7. O'Keefe GJ, Saunderson TH, Ng S, et al. Radiation dosimetry of beta-amyloid tracers 11C-PiB and 18F-BAY94-9172. *J Nucl Med*. 2009;50:309-15.
8. Quinn B, Dauer Z, Pandit-Taskar N, Schoder H, Dauer LT. Radiation dosimetry of 18F-FDG PET/CT: incorporating exam-specific parameters in dose estimates. *BMC Med Imaging*. 2016;16:41.
9. Scheinin NM, Tolvanen TK, Wilson IA, Arponen EM, Nagren KA, Rinne JO. Biodistribution and radiation dosimetry of the amyloid imaging agent 11C-PIB in humans. *J Nucl Med*. 2007;48:128-33.
10. Tu Z, Mach RH. C-11 radiochemistry in cancer imaging applications. *Curr Top Med Chem*. 2010;10:1060-95.
11. Henley D, Lightman S, Carrell R. Cortisol and CBG-Getting cortisol to the right place at the right time. *Pharmacol Ther*. 2016;166:128-35.
12. Truillet C, Parker MFL, Huynh LT, et al. Measuring glucocorticoid receptor expression in vivo with PET. *Oncotarget*. 2018;9:20399-20408.
13. Rathkopf DE, Morris MJ, Fox JJ, et al. Phase I study of ARN-509, a novel antiandrogen, in the treatment of castration-resistant prostate cancer. *J Clin Oncol*. 2013;31:3525-30.
14. Kurland BF, Peterson LM, Lee JH, et al. Estrogen receptor binding (18F-FES PET) and glycolytic activity (18F-FDG PET) predict progression-free survival on endocrine therapy in patients with ER+ breast cancer. *Clin Cancer Res*. 2017;23:407-415.
15. Rew Y, Du X, Eksterowicz J, et al. Discovery of a potent and selective steroidal glucocorticoid receptor antagonist (ORIC-101). *J Med Chem*. 2018;61:7767-7784.

Figure 1. A summary of the synthesis and in vivo assessment of (\pm)- ^{11}C -YJH08 biodistribution. A. A summary of the radiosynthesis of (\pm)- ^{11}C -YJH08. **B.** Semipreparative UV HPLC traces showing the retention of phenol precursor (**7**) and cold (\pm)-YJH08 (**8**). Below is shown the UV trace of the complex reaction mixture at 10 min and the corresponding radioactive trace. The major peak at 10.12 min corresponds to the product, (\pm)- ^{11}C -YJH08. **C.** A time activity curve from a dynamic PET scan in a wild type male C57Bl6/J mouse shows that (\pm)- ^{11}C -YJH08 rapidly cleared from the serum, as expected, and the primary mode of clearance appeared to be hepatobiliary. The data also show saturable radiotracer accumulation in the brain and brown fat, two GR rich tissues. At right are shown representative sagittal and coronal slices of the mouse injected with (\pm)- ^{11}C -YJH08 PET/CT.

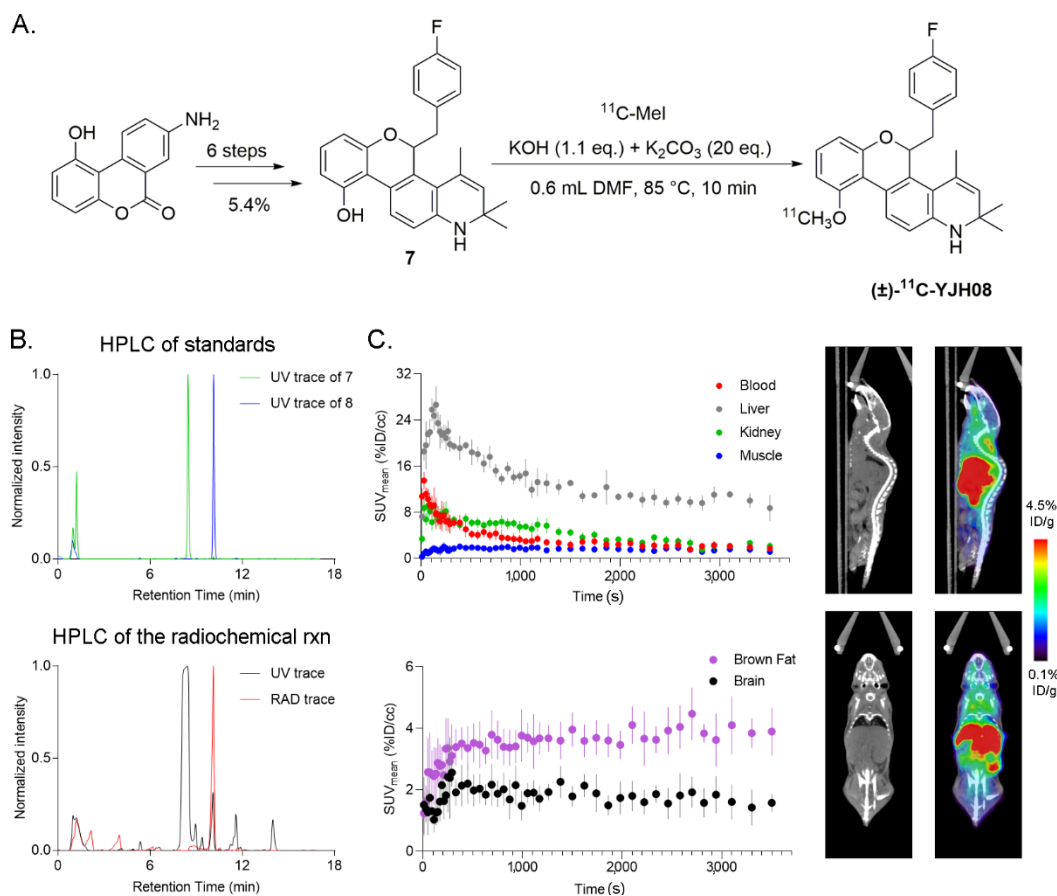


Figure 2. In vivo blocking studies reveal that (\pm)- ^{11}C -YJH08 specifically binds GR in vivo.

A. Biodistribution data collected 20 min post injection showing the suppression of (\pm)- ^{11}C -YJH08 uptake in several mouse tissues by dexamethasone (Dex, n = 5/arm). Dex was administered via two routes involving oral gavage of 50 mg/kg for three days prior to radiotracer injection or administration of a water-soluble dexamethasone-cyclodextrin (CD) complex via intraperitoneal injection at 10 mg/kg one hour prior to radiotracer injection. *P<0.05. At right is shown the blocking data observed in the brain. *P<0.01 **B.** The percent changes in radiotracer uptake per tissue among mice exposed to dexamethasone or Dex-CD versus vehicle. **C.** Representative CT and PET/CT images showing the suppression of (\pm)- ^{11}C -YJH08 binding in selected organs in vivo by Dex treatment.

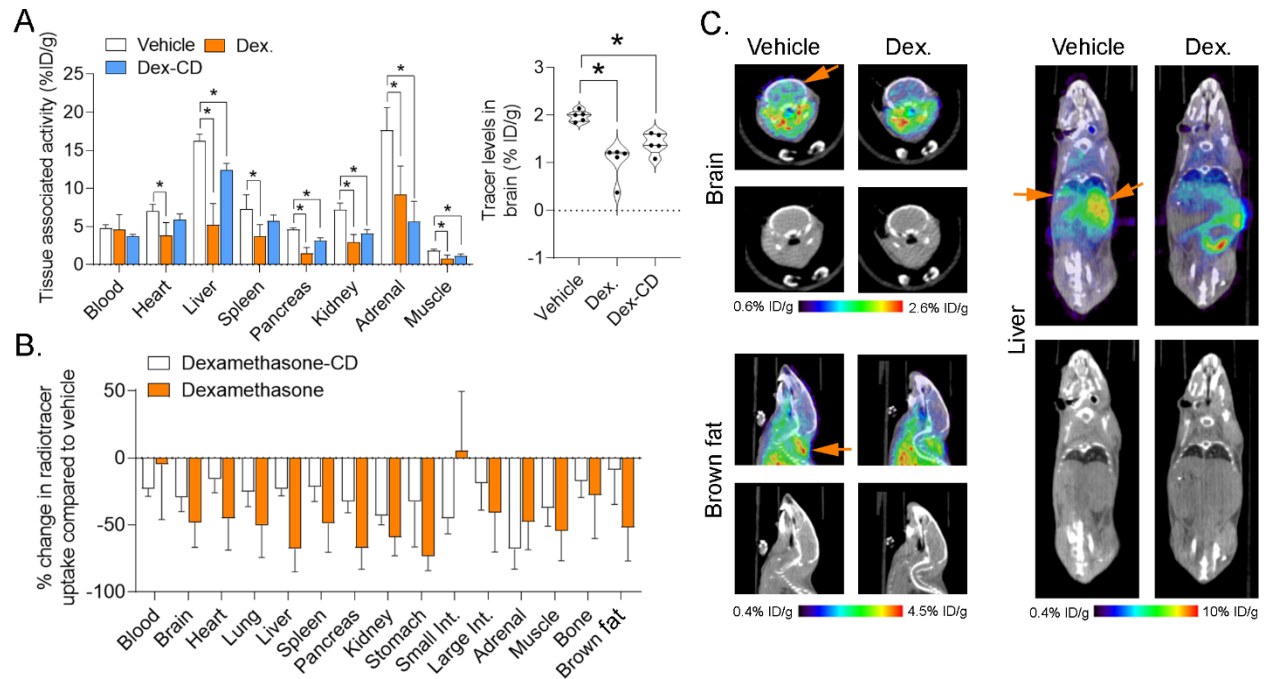
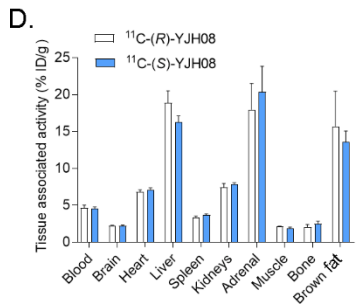
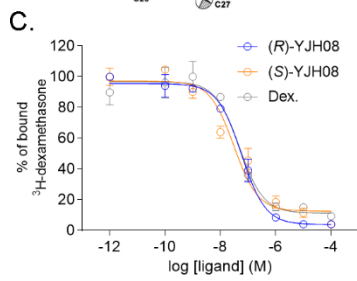
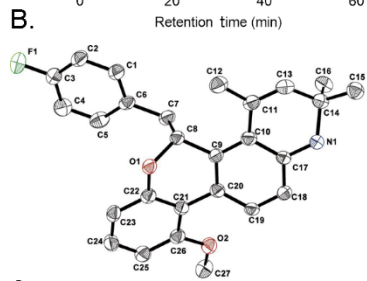
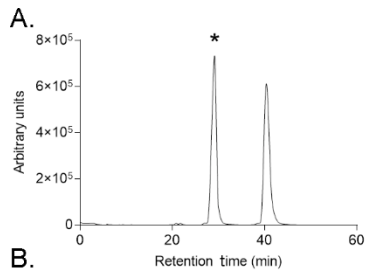


Figure 3. Resolution and analysis of the *R/S* YJH08 enantiomers reveals similar affinity for GR in vitro and biodistribution patterns in vivo. **A.** An HPLC trace over a chiral stationary phase shows the separation of racemic YJH08 to provide *R* and *S* isomers. The starred peaked at 29.1 min was isolated in and recrystallized in hexanes to give a single crystal. **B.** An Ortep plot showing the absolute conformation of the crystal, which was the (*R*) enantiomer of YJH08. Thermal ellipsoids are drawn at 40% probability. **C.** ³H-dexamethasone displacement curves on DU145 cells showing the relative affinities of (*R*)-YJH08, (*S*)-YJH08 and dexamethasone. Each ligand has an affinity <5 nM, and are equipotent. R² values for curve fitting were 0.99 (*R*), 0.94 (*S*), and 0.97 (dexamethasone). **D.** Mouse biodistribution data showing the tissue uptake of *R*- and *S*-¹¹C-YJH08. The data were acquired 20 min post injection in male C57Bl6/J mice. **E.** Structures of the (*S*) and (*R*) enantiomers of YJH08. The bonds are colored coded to enable the distinction of the small molecule structure in the ligand binding domain of GR. Below each enantiomer are the results of a molecular dynamics simulation to identify the lowest energy interaction between the ligand binding domain of GR and the respective enantiomer. Receptor side chains within 5 Å of the respective YJH08 enantiomer are shown. For clarity, two docked poses are shown for each ligand/receptor complex. At bottom is shown a schematic representation of the docked pose for each enantiomer within the GR ligand binding domain is shown to highlight the amino acids within 5 Å of the respective enantiomer.



E.

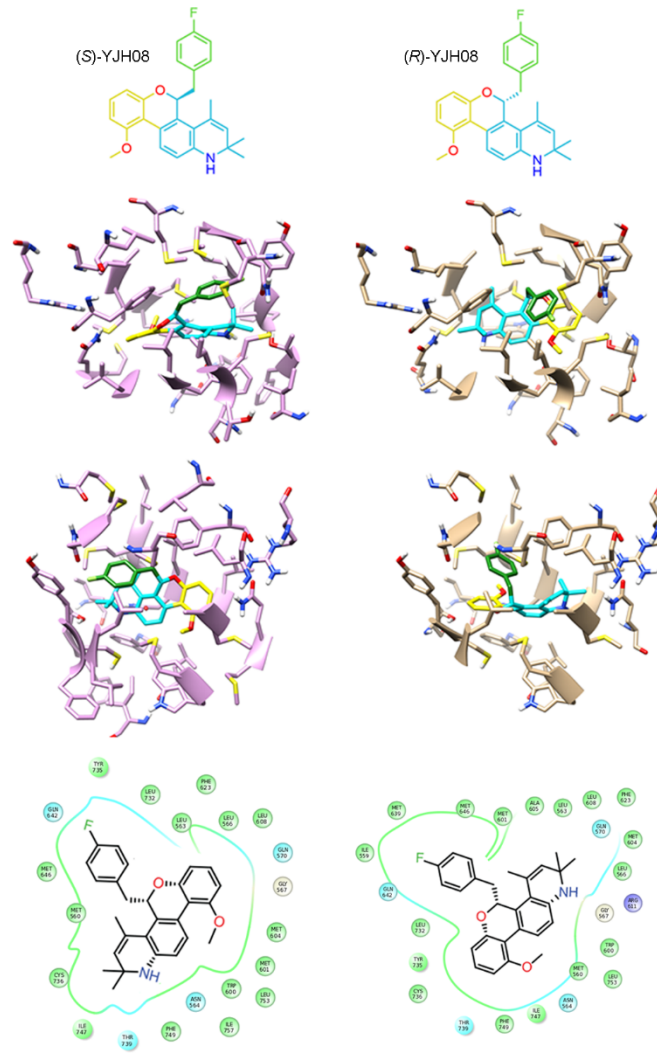


Figure 4. Biodistribution studies with the analogue ^{11}C -YJH02 show the importance of the 4-fluoro-benzyl motif to specific GR binding *in vivo*. **A.** A schematic of the synthesis of ^{11}C -YJH02. **B.** Biodistribution data showing the tissue uptake of ^{11}C -YJH02 in mice. The data are showing tracer distribution in mice that received vehicle or dexamethasone-cyclodextrin at 10 mg/kg via intraperitoneal injection 1 hour prior to radiotracer injection. Radiotracer uptake was evaluated 20 min post injection. * $P < 0.01$ **C.** A comparison of ^{11}C -YJH02 and (\pm)- ^{11}C -YJH08 uptake among tissues in normal mice. The uptake of ^{11}C -YJH02 was generally lower than (\pm)- ^{11}C -YJH08. * $P < 0.05$

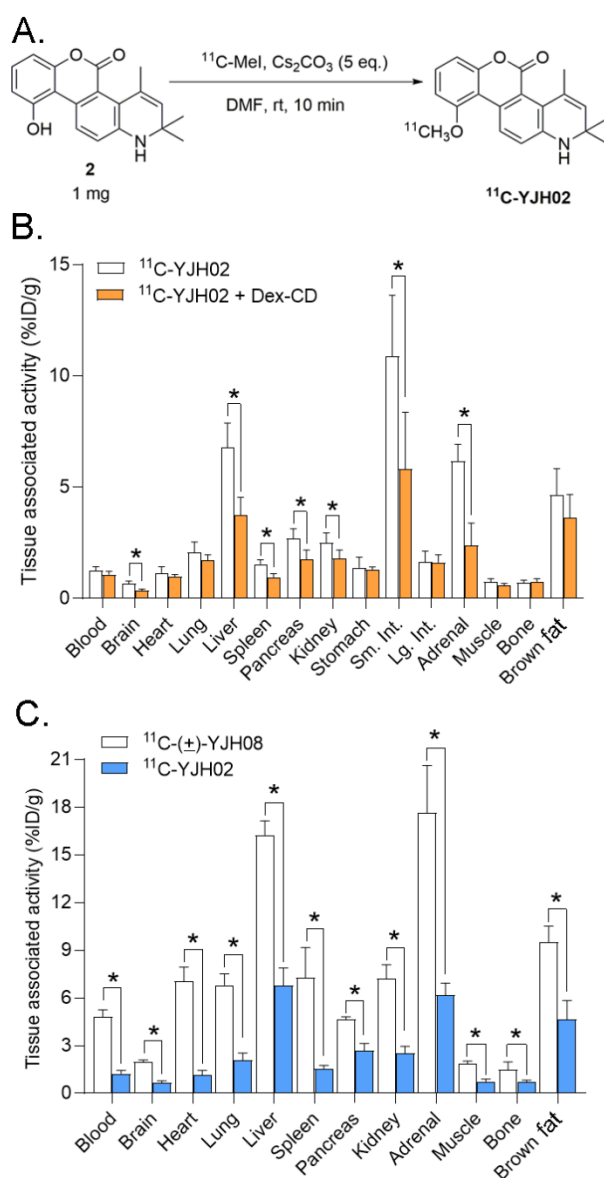
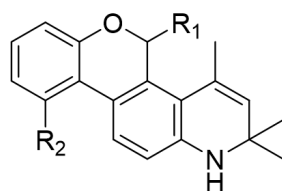


Table 1. A summary of the biodistribution data for (\pm)- ^{11}C -YJH08 versus (\pm)- ^{18}F -YJH08. The data were collected in intact male C57Bl6/J mice at 20 min post injection. The data for (\pm)- ^{18}F -YJH08 were previously reported(6).

Tissue	(\pm)-^{11}C-YJH08 (%ID/g)	(\pm)-^{18}F-YJH08 (%ID/g)
Blood	2.25 \pm 0.21	2.22 \pm 0.14
Brain	1.81 \pm 0.17	1.93 \pm 0.07
Heart	4.47 \pm 0.43	4.15 \pm 0.31
Liver	12.19 \pm 1.22	11.08 \pm 0.92
Spleen	2.22 \pm 0.33	2.46 \pm 0.53
Kidneys	5.82 \pm 0.28	5.79 \pm 1.07
Supraspinal brown fat depot	9.8 \pm 2.83	9.01 \pm 2.07
Adrenal gland	13.88 \pm 7.15	12.19 \pm 6.46
Muscle	1.53 \pm 0.13	1.53 \pm 0.12
Bone	1.19 \pm 0.13	1.3 \pm 0.23

Table 2. A summary of the K_i , 95% confidence intervals, and the coefficient of determination for YJH08. The data were calculated from ^3H -dexamethasone displacement assay on cells. The K_i were calculated using a one site K_i fit nonlinear regression with Prism v8.0. The data are representative of two independent assays.



YJH01-05

Ligand	R ₁	R ₂	K _i (nM)	95% CI	R ²
YJH01	=O	OH	2.35	1.15 – 4.59	0.96
YJH02	=O	OMe	2.67	1.32 – 5.28	0.93
YJH03	OH	OMe	6.51	3.52 – 12.8	0.94
YJH04	OMe	OMe	6.22	1.00 – 3.85	0.96
YJH05	PhCH ₂	OMe	0.326	0.112 – 0.789	0.92

Table 3. A summary of the mouse dosimetry data for (\pm)- ^{11}C -YJH08. The values were calculated from a 90 min dynamic PET acquisition in intact male or female C57Bl6/J mice.

Organ	Absorbed Dose (mGy/MBq) or Equivalent Dose (mSv/MBq)	
	Adult male (73 kg)	Adult female (60 kg)
Adrenals	0.00533 \pm 0.000748	0.00578 \pm 0.000156
Brain	0.00140 \pm 0.000022	0.00229 \pm 0.000078
Breasts		0.00286 \pm 0.000129
Esophagus	0.00831 \pm 0.004249	0.00544 \pm 0.000439
Eyes	0.00194 \pm 0.000092	0.00223 \pm 0.000061
Gallbladder Wall	0.00602 \pm 0.000876	0.00459 \pm 0.000041
Left colon	0.00374 \pm 0.000769	0.00437 \pm 0.000314
Small Intestine	0.00325 \pm 0.000446	0.00325 \pm 0.000114
Stomach Wall	0.01628 \pm 0.005962	0.01925 \pm 0.002944
Right colon	0.00367 \pm 0.000548	0.00339 \pm 0.000070
Rectum	0.00249 \pm 0.000093	0.00280 \pm 0.000087
Heart Wall	0.06753 \pm 0.050725	0.02570 \pm 0.005677
Kidneys	0.00714 \pm 0.000174	0.00785 \pm 0.001344
Liver	0.01568 \pm 0.001377	0.01863 \pm 0.001258
Lungs	0.01350 \pm 0.011132	0.00909 \pm 0.000339
Pancreas	0.00665 \pm 0.002374	0.00545 \pm 0.000182
Ovaries		0.00288 \pm 0.000090
Prostate	0.00250 \pm 0.000105	
Salivary Glands	0.00226 \pm 0.000156	0.00241 \pm 0.000068
Red Marrow	0.00310 \pm 0.000771	0.00289 \pm 0.000101
Osteogenic Cells	0.00223 \pm 0.000391	0.00217 \pm 0.000069
Spleen	0.00378 \pm 0.000828	0.00432 \pm 0.000300
Testes	0.00204 \pm 0.000046	
Thymus	0.01004 \pm 0.005999	0.00498 \pm 0.000454
Thyroid	0.00355 \pm 0.001070	0.00297 \pm 0.000118
Urinary Bladder Wall	0.00247 \pm 0.000136	0.00288 \pm 0.000114
Uterus		0.00284 \pm 0.000085
Total Body	0.00355 \pm 0.000856	0.00366 \pm 0.000121
Effective Dose (mSv/MBq)	0.00673 \pm 0.002757	0.00649 \pm 0.000433

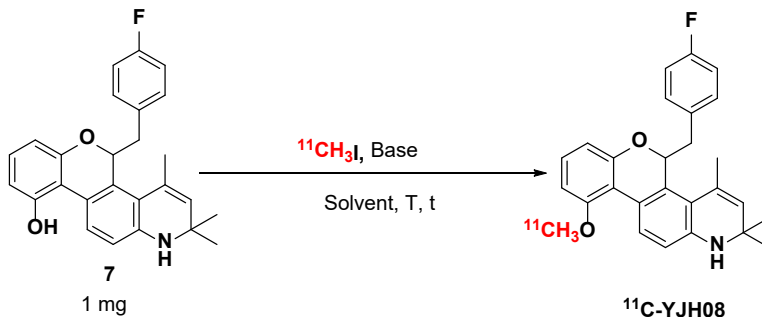
Supplemental Material for
The synthesis and structural requirements for measuring glucocorticoid receptor
expression in vivo with (±)-¹¹C-YJH08 PET

Table of Contents

Supplemental Tables	2
Supplemental figures.....	8
Supplemental Methods.....	Error! Bookmark not defined.
Synthesis and Radiochemistry.....	16
General Procedures:	16
Instrumentation:	16
Synthetic Schemes and Procedures	Error! Bookmark not defined.
Copies of NMR spectrum.....	24

Supplemental Tables

Supplemental Table 1: A summary of the radiomethylation conditions screened to synthesize (\pm)- ^{11}C -YJH08 from the phenol precursor **7**. [a]



Entry	Solvent	Base	t (°C)	Time (min)	RCY (%)
1	DMSO	KOH (50 eq.)	rt	5	1.0 \pm 0.8
2	DMSO	KOH (50 eq.)	80	10	0.5 \pm 0.1
3	DMF	KOH (50 eq.)	100	10	6.6 \pm 2.3
4	DMF	KOH (1.0 eq.) + K ₂ CO ₃ (20 eq.)	100	10	12.0 \pm 3.6
5	DMF	KOH (1.1 eq.) + K ₂ CO ₃ (20 eq.)	85	10	51.7 \pm 4.7

[a] Radiomethylation of precursor **7** by $^{11}\text{CH}_3\text{I}$ using different base. Conserved reaction conditions: 1 mg of precursor **7**, 20 μL base solution, air, 0.6 mL of DMF. RCY = Radiochemical yield based on radio HPLC; each experiment was performed in triplicate.

Supplemental Table 2. Results from duplicate plasma protein binding assays with (±)-YJH08 in mouse or human serum. Propranolol was included as a reference standard.

Species	Compound	Concentration (μM)	% Bound	% Bound Average	%Recovery
Human	Propranolol	2	64.57	64.57	104.13
			64.56		
	(±)-YJH08	2	>99.99	>99.99	97.56
			>99.99		
Mouse	Propranolol	2	78.25	78.00	105.82
			77.74		
	(±)-YJH08	2	>99.99	>99.99	100.31
			>99.99		

Supplemental Table 3. A tabular representation of the biodistribution data collected 20 minutes after injection of (\pm)- ^{11}C -YJH08 among three treatment arms receiving (1) vehicle, (2) dexamethasone at 50 mg/kg via gavage once daily for three days, and (3) one intraperitoneal injection of the water soluble dexamethasone-cyclodextrin complex at 10 mg/kg one hour prior to radiotracer administration. The P value indicates the result of an unpaired, two-tailed Student's t test between the respective treatment group and vehicle (n = 5/group).

Tissue	Vehicle	Dexamethasone (50 mg/kg)		Dex-CD (10 mg/kg)	
	Mean \pm SD	Mean \pm SD	P value	Mean \pm SD	P value
Blood	4.82 \pm 0.4	4.58 \pm 1.9	0.8	3.72 \pm 0.2	0.001
Brain	1.98 \pm 0.1	1.02 \pm 0.3	0.002	1.40 \pm 0.2	0.001
Heart	7.06 \pm 0.8	3.86 \pm 1.6	0.008	5.95 \pm 0.7	0.06
Lung	6.80 \pm 0.7	3.39 \pm 1.6	0.006	5.09 \pm 0.7	0.006
Liver	16.25 \pm 0.8	5.22 \pm 2.7	0.0004	12.47 \pm 0.8	0.0001
Spleen	7.28 \pm 1.8	3.71 \pm 1.5	0.012	5.72 \pm 0.7	0.14
Pancreas	4.64 \pm 0.1	1.52 \pm 0.7	0.0004	3.14 \pm 0.3	0.0003
Kidney	7.22 \pm 0.8	2.96 \pm 0.9	0.0001	4.11 \pm 0.4	0.0003
Stomach	2.62 \pm 1.5	0.71 \pm 0.2	0.04	1.79 \pm 0.8	0.3
Sm. Int.	28.72 \pm 14.5	30.24 \pm 12.7	0.8	15.72 \pm 3.2	0.1
Lg. Int.	1.70 \pm 0.3	1.01 \pm 0.5	0.03	1.38 \pm 0.3	0.1
Adrenal	17.63 \pm 2.9	9.24 \pm 3.6	0.004	5.67 \pm 2.6	0.0001
Muscle	1.85 \pm 0.1	0.84 \pm 0.4	0.003	1.16 \pm 0.2	0.001
Bone	1.46 \pm 0.5	1.06 \pm 0.4	0.23	1.95 \pm 1.6	0.5
Brown Fat	9.52 \pm 0.9	4.58 \pm 2.3	0.006	8.68 \pm 2.4	0.5

Supplemental Table 4. A tabular representation of the biodistribution data collected 20 minutes after injection of (\pm)- ^{11}C -YJH08 in intact or adrenalectomized (ADREX) mice. The P value indicates the result of an unpaired, two-tailed Student's t test between the two arms (n = 4/group).

Tissue	Intact	ADREX	P value
Blood	2.25 \pm 0.21	2.79 \pm 0.54	0.105941
Brain	1.81 \pm 0.17	2.28 \pm 0.46	0.004892
Heart	4.47 \pm 0.43	5.63 \pm 0.94	0.065629
Liver	12.19 \pm 1.22	15.21 \pm 3.39	0.144531
Spleen	2.22 \pm 0.33	2.88 \pm 0.68	0.130557
Kidneys	5.82 \pm 0.28	6.88 \pm 1.52	0.219835
Muscle	1.53 \pm 0.13	2.32 \pm 0.5	0.021735
Bone	1.19 \pm 0.13	2.03 \pm 0.4	0.007503
Supraspinal BAT	9.8 \pm 2.83	12.01 \pm 3.54	0.069191
Adrenal Gland	13.88 \pm 7.15	N/A	N/A

Supplemental Table 5: Crystal data and structure refinement for (*R*) - YJH08.

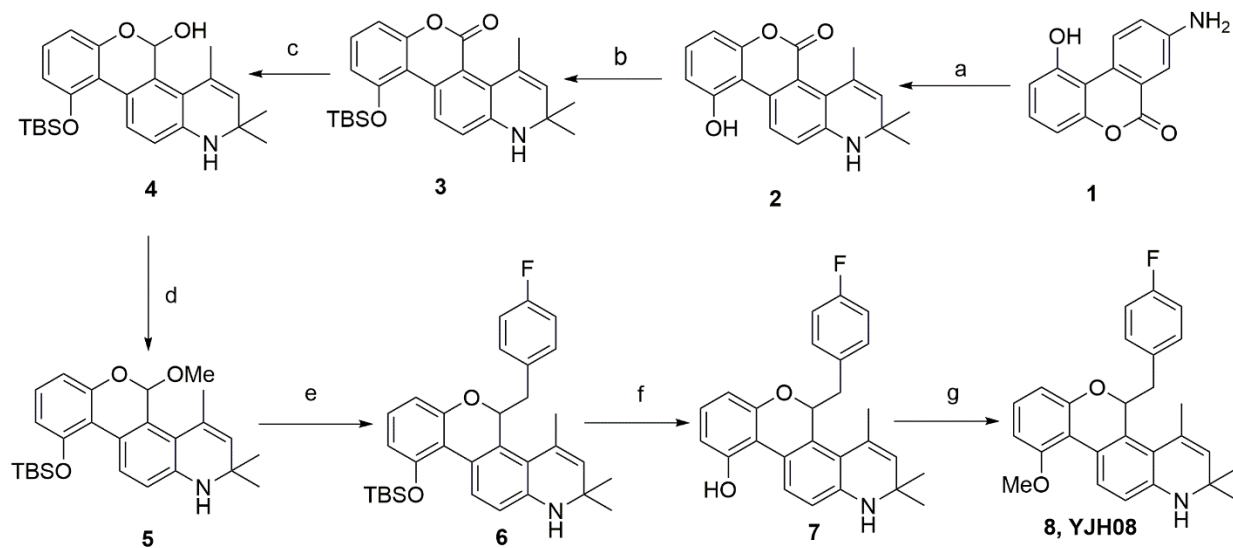
Identification code	(<i>R</i>) - YJH08
Empirical formula	C ₂₇ H ₂₆ F N O ₂
Formula weight	415.49
Temperature	100(2) K
Wavelength	1.54184 Å
Crystal system	Monoclinic
Space group	P 21
Unit cell dimensions	a = 7.87481(4) Å $\alpha = 90^\circ$. b = 16.99503(8) Å $\beta = 90.0427(4)^\circ$. c = 15.53997(7) Å $\gamma = 90^\circ$.
Volume	2079.755(18) Å ³
Z	4
Density (calculated)	1.327 Mg/m ³
Absorption coefficient	0.716 mm ⁻¹
F(000)	880
Crystal size	0.220 x 0.150 x 0.100 mm ³
Theta range for data collection	2.844 to 74.496°.
Index ranges	-9 ≤ h ≤ 9, -21 ≤ k ≤ 21, -19 ≤ l ≤ 19
Reflections collected	119512
Independent reflections	8504 [R(int) = 0.0663]
Completeness to theta = 74.000°	100.0 %
Absorption correction	Semi-empirical from equivalents
Max. and min. transmission	1.00000 and 0.90694
Refinement method	Full-matrix least-squares on F ²
Data / restraints / parameters	8504 / 1 / 576
Goodness-of-fit on F ²	1.047
Final R indices [I > 2σ(I)]	R1 = 0.0351, wR2 = 0.0951
R indices (all data)	R1 = 0.0354, wR2 = 0.0954
Absolute structure parameter	0.01(4)
Extinction coefficient	n/a
Largest diff. peak and hole	0.224 and -0.205 e.Å ⁻³

Supplemental Table 6. A tabular representation of the biodistribution data collected 20 minutes after injection of ^{11}C -YJH02 among two treatment arms receiving vehicle or one intraperitoneal injection of the water-soluble dexamethasone-cyclodextrin complex at 10 mg/kg one hour prior to radiotracer administration. The P value indicates the result of an unpaired, two-tailed Student's t test between the respective treatment group and vehicle (n = 5/group).

Tissue	Vehicle	Dex-CD (10 mg/kg)	
	Mean \pm SD	Mean \pm SD	P value
Blood	1.24 \pm 0.1	1.07 \pm 0.1	0.1
Brain	0.66 \pm 0.1	0.34 \pm 0.07	0.001
Heart	1.15 \pm 0.2	0.97 \pm 0.1	0.2
Lung	2.07 \pm 0.4	1.71 \pm 0.2	0.1
Liver	6.78 \pm 1.1	3.75 \pm 0.8	0.0001
Spleen	1.55 \pm 0.1	0.76 \pm 0.1	0.008
Pancreas	2.70 \pm 0.4	1.76 \pm 0.4	0.008
Kidney	1.38 \pm 0.4	1.28 \pm 0.1	0.06
Stomach	2.51 \pm 0.4	1.81 \pm 0.3	0.02
Sm. Int.	10.88 \pm 2.7	5.80 \pm 2.5	0.01
Lg. Int.	1.63 \pm 0.4	1.06 \pm 0.3	0.97
Adrenal	6.17 \pm 0.7	2.37 \pm 1.0	0.0009
Muscle	0.74 \pm 0.1	0.57 \pm 0.1	0.07
Bone	0.70 \pm 0.1	0.76 \pm 0.1	0.4
Brown Fat	4.65 \pm 1.1	3.64 \pm 1.0	0.18

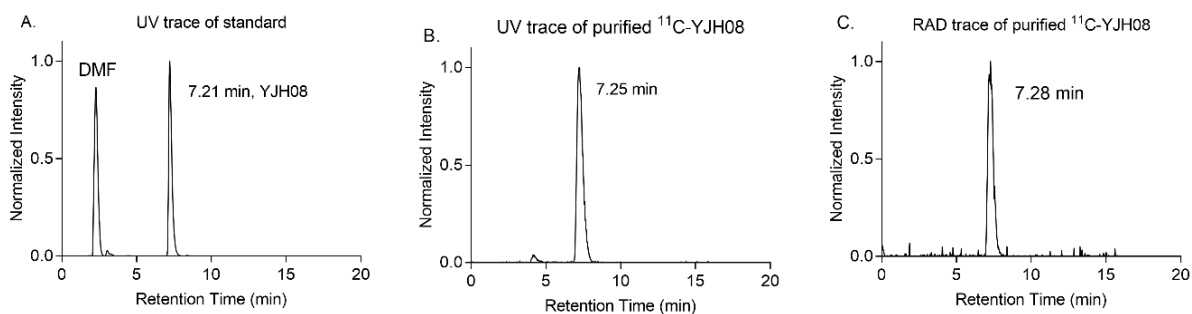
Supplemental figures

Supplemental Fig. 1 Synthesis of YJH08 and the radiochemistry precursor 7.

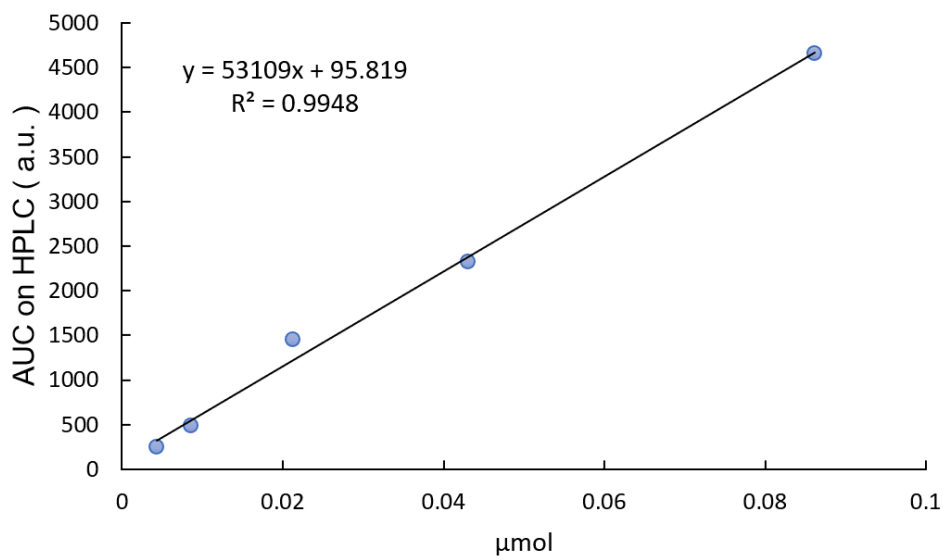


Reagents and conditions: (a) 0.4 eq I_2 , anhydrous aceton, 105°C, 41%; (b) TBSCl, Imidazole, THF r.t., 58%; (c) 1M DIBAL in hexanes, anhydrous CH_2Cl_2 , -78°C, 80%; (d) *p*-TsOH·H₂O, MeOH, 0 °C to rt, 0.5h, 81%; (e) 0.25M 4-Fluorobenzylmagnesium chloride in THF, $BF_3 \cdot Et_2O$; 52%; (f) TBAF, THF, r.t. 68%; (g) MeI, CS_2CO_3 , DMF, r.t., 99%.

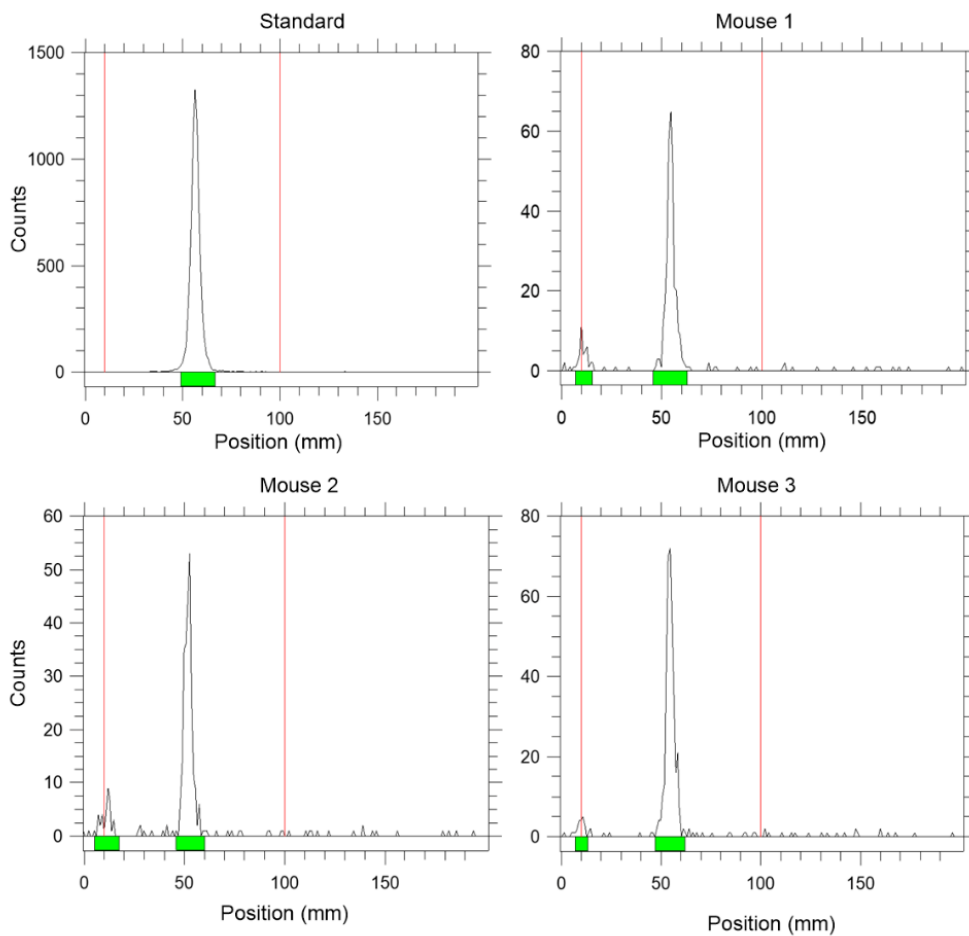
Supplemental Fig. 2 Verification of the purity of (\pm)- ^{11}C -YJH08 on analytical HPLC using an isocratic gradient. At left is shown the UV trace of the purified YJH08 standard material. The peak was resolved on a Waters column (4.6 x 150 mm) with 3.5 μM C18 beads using an isocratic mobile phase of 80% CH_3CN in H_2O with 0.1% formic acid. The flow rate was 1 mL/min. Using the same conditions, the purified product of the radiomethylation reaction was shown to co-elute with the standard on UV (middle) and rad-HPLC (right).



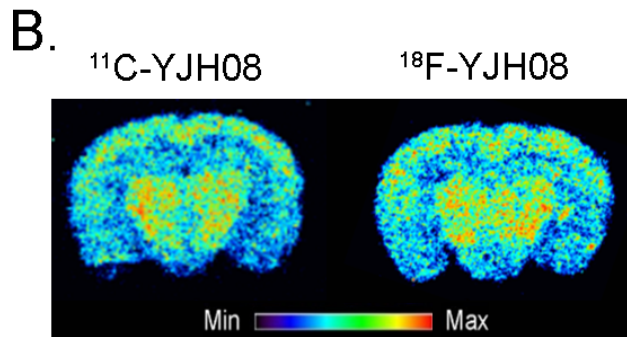
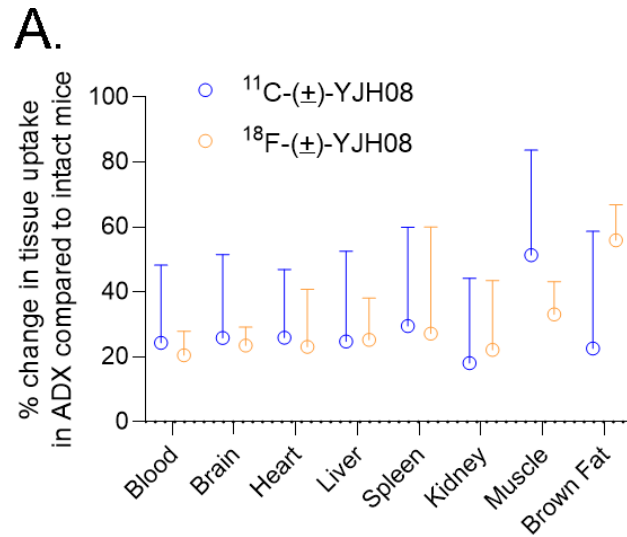
Supplemental Fig. 3. A plot of the standard curve used to calculate specific activity of (\pm)- ^{11}C -YJH08. Known quantities of YJH08 were resolved on the semi-prep HPLC schema used to purify the complex (\pm)- ^{11}C -YJH08 reaction mixture. The corresponding areas under the curve (AUC) were determined to calculate the concentration of YJH08 co-eluting with (\pm)- ^{11}C -YJH08. The specific activity was subsequently calculated using the decay corrected amount of radioactivity found on the HPLC.



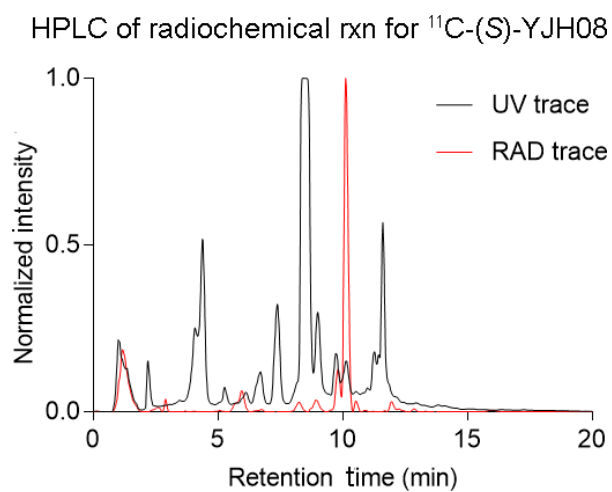
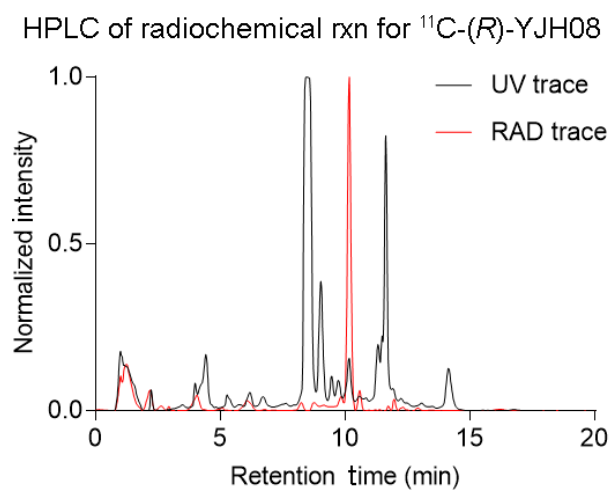
Supplemental Fig. 4 ITLC data showing the serum stability of (\pm)- ^{11}C -YJH08 in vivo. (\pm)- ^{11}C -YJH08 was injected into wild type C57Bl6/J mice ($n = 3$) and blood was harvested at 30 minutes post injection. Blood was directly spotted onto a TLC plate and resolved using a 10% ethyl acetate in hexanes as mobile phase. Area under the curve analysis showed the peak co-migrating with (\pm)- ^{11}C -YJH08 standard to represent $90.45 \pm 4.03\%$ ($n = 3$) % of total activity on the ITLC trace.



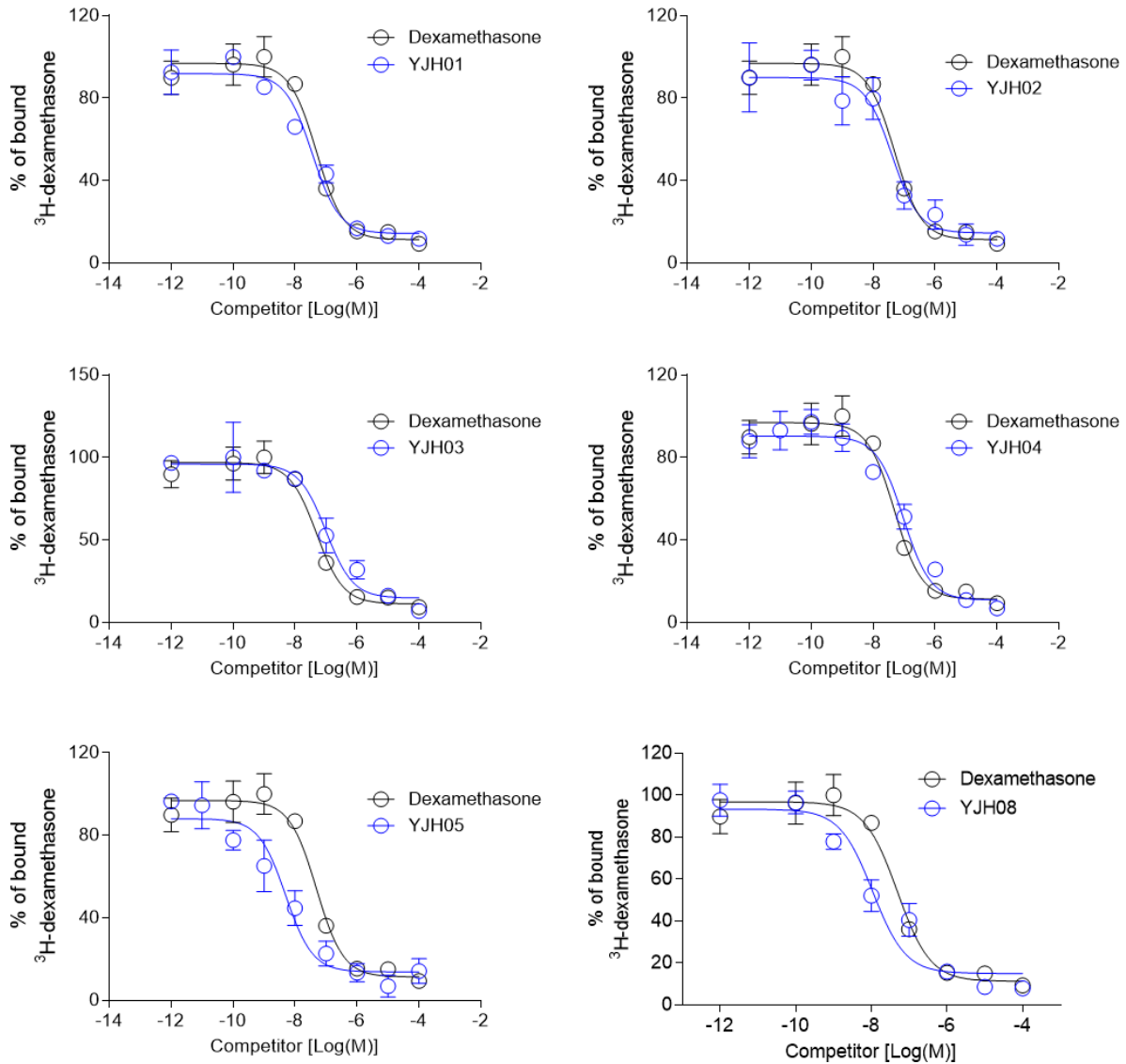
Supplemental Fig. 5. A. A comparison of the percent change in radiotracer uptake between adrenalectomized and intact mice for (\pm)- ^{11}C -YJH08 and (\pm)- ^{18}F -YJH08. Both data sets were collected at 20 minutes post injection in C57Bl6/J mice. **B.** Digital autoradiography showing the (\pm)- ^{11}C -YJH08 and (\pm)- ^{18}F -YJH08 have qualitatively similar distribution in brain. The slices are -2.33 mm from bregma.



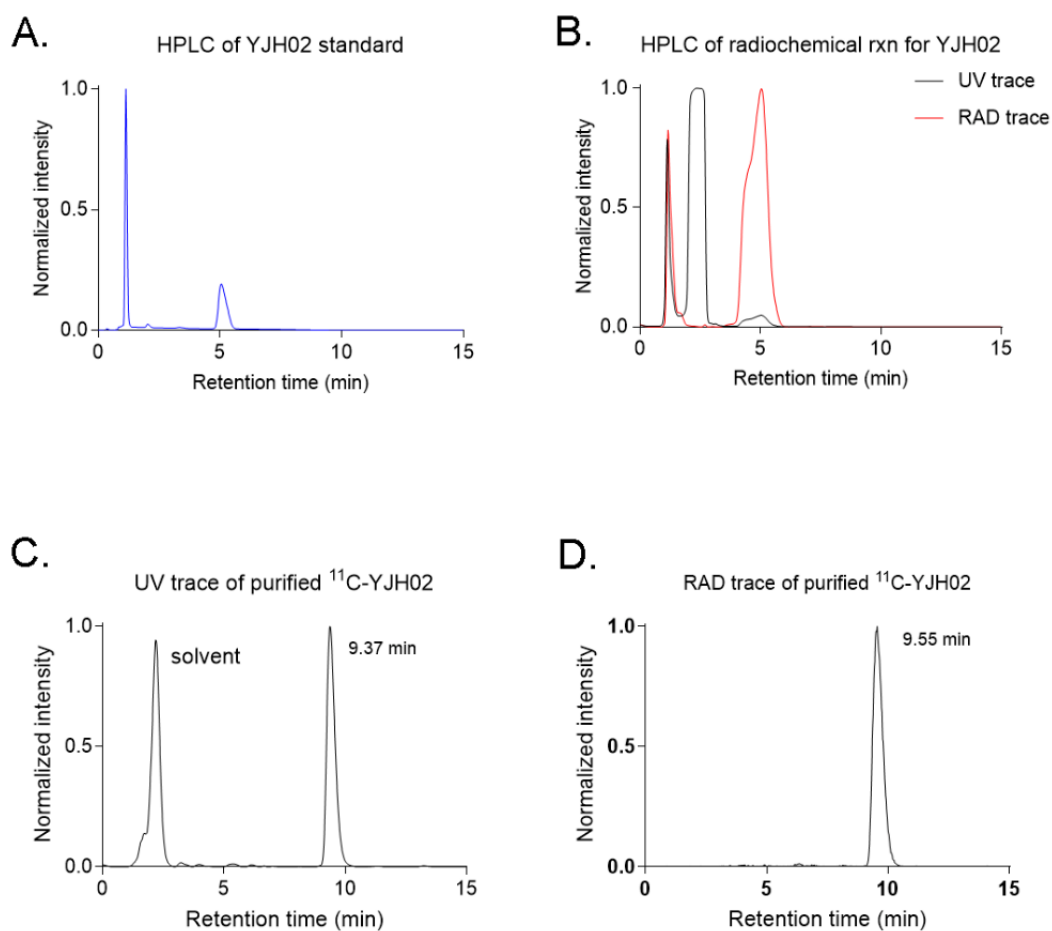
Supplemental Fig. 6. Semipreparative HPLC traces showing the synthesis of the enantiopure ^{11}C -YJH08.



Supplemental Fig. 7. Ligand displacement curves showing the dose dependent interaction between the indicated YH08 analogue and GR. The assays were conducted on HEK293 cells transiently overexpressing wild type full length GR alpha. ³H-dexamethasone and the cold ligand were incubated on cells for 10 min prior to harvesting and measuring activity. The data were fit with Prism, and are representative of two independent experiments.



Supplemental Fig. 8. A. A semipreparative UV HPLC traces showing the retention the YJH02. **B.** A stacked semipreparative RAD-HPLC trace of the complex reaction mixture to prepare ^{11}C -YJH02 at 10 min and the corresponding trace collected based on radiation detector. A strong product peak at 5 min in RAD-HPLC that aligned with the UV standard peak for YJH02. **C.** An analytical trace of the reinjected product after collection off the semiprep HPLC shows one peak at 9.3 min. **D.** A RAD tracer of the reinjected product after collection off the semiprep HPLC shows one peak at 9.5 min that co-elutes with the UV peak.



Synthesis and Radiochemistry

General Procedures:

All reactions were performed under an Ar(g) atmosphere using anhydrous solvents obtained from commercial suppliers in oven-dried round-bottom flasks containing Teflon coated stirrer bars, unless otherwise noted. All anhydrous solvents used were purchased from Sigma-Aldrich and used without further purification. Solvents to be employed in flash column chromatography and reaction work-up procedures were purchased from either Sigma-Aldrich or Fisher Scientific. All other reagents were obtained commercially and used without further purification, unless otherwise stated. Air and/or moisture sensitive reagents were transferred via syringe and were introduced into reaction vessels through rubber septa. Reactions were monitored using thin layer chromatography (TLC), performed on 0.25-mm EMD pre-coated glass-backed silica gel 60 F-254 plates. Column chromatography was performed on Silicycle Sili-prep cartridges using a Biotage Isolera Four automated flash chromatography system. Compounds were visualized under UV light or through staining with permanganate, or most preferably for trioxolane analogs, Seebach's "Magic" stain (composed of the following: 2.5 g phosphomolybdic acid, 1.0 g cerium sulfate, 6 mL concentrated sulfuric acid, and 94 mL water). Solution containing crude reaction mixtures, as well as those solutions obtained upon work-up of the reaction, and chromatography fractions were first concentrated by rotary evaporation at temperatures under 40 °C, at 20 Torr then subsequently placed under Hi-Vac at 0.5 Torr unless otherwise indicated. It is imperative to maintain water bath temperatures ≤ 40 °C during rotary evaporation due to the thermal instability of trioxolanes at higher temperatures.

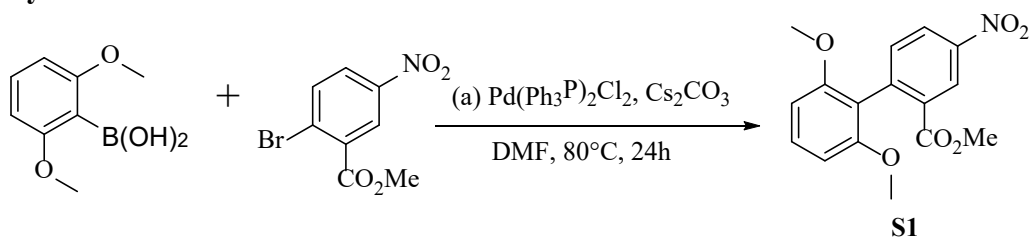
Instrumentation:

NMR spectra were recorded on a Bruker Advance III 400 MHz spectrometer at the UCSF NMR lab, and spectra were analyzed using Mestrelab software. Data for ^1H NMR spectra are reported in terms of chemical shift (δ , ppm), multiplicity, coupling constant (Hz), and integration. Data for ^{13}C NMR spectra are reported in terms of chemical shift (δ , ppm), with multiplicity and coupling constants in the case of C–F coupling. The following abbreviations are used to denote the multiplicities: s = singlet; d = doublet; dd = doublet of doublets; dt = doublet of triplets; dq = doublet of quartets; ddd = doublet of doublet of doublets; t = triplet; td = triplet of doublets; tt = triplet of triplets; q = quartet; qd = quartet of doublets; quin = quintet; sex = sextet; m = multiplet. LC-MS and compound purity were determined using Waters Micromass ZQ 4000, equipped with a Waters 2795 Separation Module, Waters 2996 Photodiode Array Detector, and a Waters 2424 ELSD. Separations were carried out with an XBridge BEH C18, 3.5 μm , 4.6 x 20 mm column, at ambient temperature (unregulated) using a mobile phase of water-methanol containing a constant 0.1 % formic acid. High resolution mass spectra were recorded at the QB3/Chemistry Mass

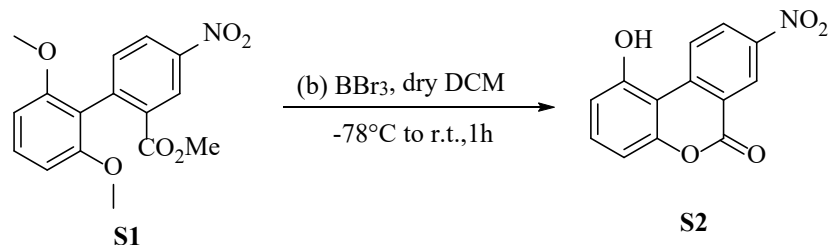
Spectrometry Facility at UC Berkeley. Crystal structure was determined at Small Molecule X-ray Crystallography Facility at UC Berkeley.

For radiochemistry, the ^{11}C -MeI (gas) was prepared and provided by the Radiopharmaceutical core facility at UCSF. ^{11}C -CO₂ was produced in target by the $^{14}\text{N}(\text{p},\text{a})^{11}\text{C}$ nuclear reaction of 17 MeV protons on N₂ at the UCSF radiopharmaceutical facility. ^{11}C -CO₂ was converted to ^{11}C -MeI using the gas-phase method on a GE FX/C Pro automated synthesis module. Semi-preparative reverse-phase HPLC purification of radiolabeled products was performed with a Waters 600 LC pump (Milford, MA) connected in series to a Shimadzu SPD-UV-Visible detector (Columbia, MD) and a gamma counting in-line radiation flow detector (Model 105a, CRA; Berkeley, CA). Separations were performed on a Phenomenex Luna® C-18(2), 10µm, 100 Å, 250 x 10 mm column at a 6 mL/min flow rate with UV detection at 254 nm. SRI PeakSimple software (version 304 – Torrance, CA) was used to acquire HPLC chromatograms. QMA light cartridges for concentrating 18F-fluoride ion and C-18 light Sep-Paks were purchased from Waters Scientific (Milford, MA).

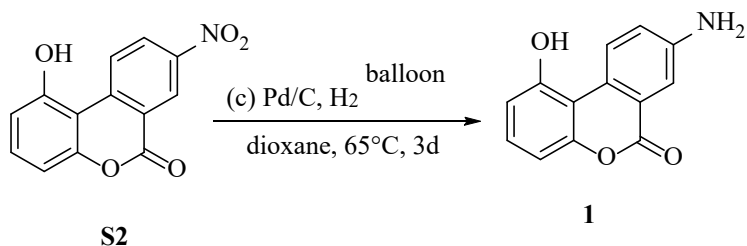
General synthetic methods



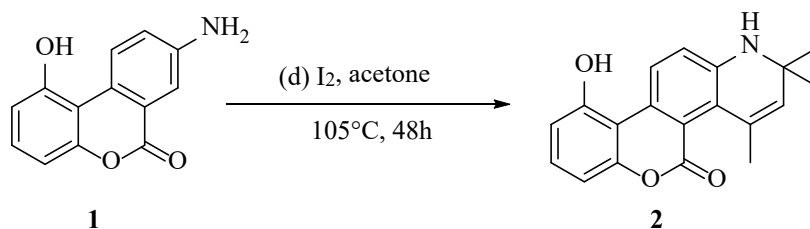
Methyl 2-(2,6-dimethoxyphenyl)-5-nitrobenzoate (S1). A dry, two-necked 500 mL round bottom flask equipped with a mechanical stirrer was sequentially charged with 1,3-dimethoxyphenylboronic acid (10.9 g, 60 mmol), methyl 5-nitro-2-bromobenzoate (12.9 g, 50 mmol), $\text{Pd}(\text{Ph}_3\text{P})_2\text{Cl}_2$ (2.1g, 3.0 mmol), Cs_2CO_3 (58.6 g, 180 mol) and dry DMF (200 mL). The reaction mixture was heated to 80°C with vigorously stirring for 24h, then cooled to r.t. and treated with water (300 mL) and EtOAc (300 mL). The layers were separated and the aqueous layer was extracted with EtOAc (100 mL \times 3). The organics portions were combined and were washed with brine (100 mL \times 3) and were dried (Na_2SO_4) and concentrated under reduced pressure to remove most of solvent, when the light yellow solid product began to precipitate from solution. Then keep the remaining mixture in a freezer (-20°C) for 2h and the light yellow product were collected by filtration and washed by hexanes to provide the **S1** (14.3 g, 45 mmol, 75%). ^1H NMR (400 MHz, DMSO) δ 8.52 (d, $J = 2.5$ Hz, 1H), 8.37 (dd, $J = 8.5, 2.5$ Hz, 1H), 7.58 (d, $J = 8.5$ Hz, 1H), 7.36 (t, $J = 8.4$ Hz, 1H), 6.75 (d, $J = 8.4$ Hz, 2H), 3.65 (s, 6H), 3.65 (s, 3H).



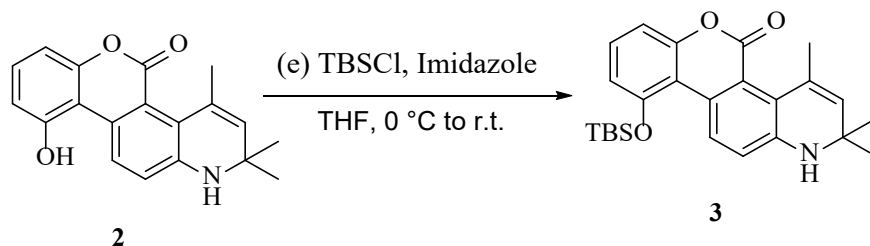
1-Hydroxy-8-nitro-6H-dibenzo[b,d]pyran-6-one (S2). A solution of **S1** (14.3 g, 45 mol) in dry CH_2Cl_2 at -78°C was slowly added BBr_3 (33.5 g, 135 mol), then remove the cold bath and warmed to r.t. The mixture form a deep red, homogenous solution, and a solid began to precipitate from solution. The mixture was stirred at r.t. for 1 h and then recooled to -78°C and quenched carefully with anhydrous MeOH (100 mL). Upon addition of MeOH, the red disappeared and a bright yellow solid precipitated from solution. The mixture was warmed to 0°C , and the yellow precipitate was collected by filtration to provide pure product **S2** (10.4 g, 40.5 mmol, 90%). ^1H NMR (400 MHz, DMSO) δ 11.48 (br, s, 1H), 9.31 (d, $J = 9.2$ Hz, 1H), 8.86 (d, $J = 2.6$ Hz, 1H), 8.66 (dd, $J = 9.2, 2.7$ Hz, 1H), 7.47 (t, $J = 8.2$ Hz, 2H), 6.96 (dd, $J = 8.3, 1.0$ Hz, 1H), 6.92 (dd, $J = 8.2, 1.1$ Hz, 1H).;



1-hydroxy-8-amino-6H-dibenzo[b,d]pyran-6-one(1); To the suspension of **S2** (10.4 g, 40.5 mmol) in dry dioxane (400 mL) at r.t. was added 10% palladium on carbon (430 mg) and the suspension mixture was heated at 65°C, treated with hydrogen using balloon. After 3d, the mixture was vacuum filtered through Celite while still hot; the filter pad was washed with hot dioxane (3 x 30 mL). The filtrate was concentrated and microcrystalline aniline precipitated from solution. The desired product was vacuum filtered and dried in vacuum to give aniline **1** (8.8 g, 38.9 mmol, 96%) as a yellow solid. ¹H NMR (400 MHz, DMSO) δ 11.45 (s, 1H), 9.25 (d, *J* = 9.1 Hz, 1H), 8.82 (s, 1H), 8.62 (dd, *J* = 9.1, 2.5 Hz, 1H), 7.44 (t, *J* = 8.2 Hz, 1H), 6.90 (dd, *J* = 14.9, 8.2 Hz, 2H), 2.08 (s, 2H).

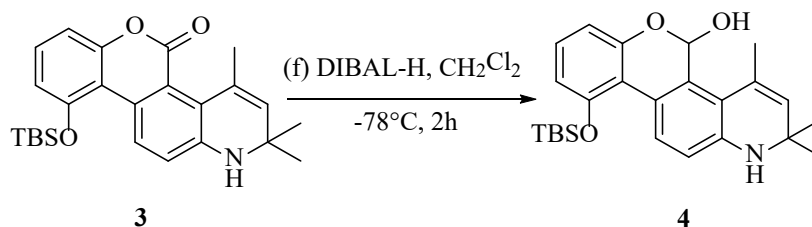


2,5-dihydro-10-hydroxy-5-oxo-2,2,4-trimethyl-1H-[1]benzopyrano [3,4-f]quinoline(2, YJH01); A solution of **1** (4.0 g, 17.6 mmol) and iodine (1.79 g, 7.04 mmol) in dry acetone (380 mL) placed into a 1L ACE glass high pressure vessel. The reaction mixture was stirred for 48 h at 105°C, cooled to room temperature (r.t.) and concentrated. The resulting brown oil was purified by flash chromatography using silica gel with 15 to 30% EtOAc in hexanes to give the desired compound **2** (2.22 g, 7.2 mmol, 41%) as a bright yellow solid. ¹H NMR (400 MHz, DMSO) δ 10.63 (br, s, 1H), 8.78 (d, *J* = 8.9 Hz, 1H), 7.50 – 6.99 (m, 2H), 6.79 (m, 3H), 5.42 (br, s, 1H), 1.93 (s, 3H), 1.22 (s, 6H). MS: Calculated for C₁₉H₁₈NO₃ 308.1281 (M+H)⁺ determined 308.1279.



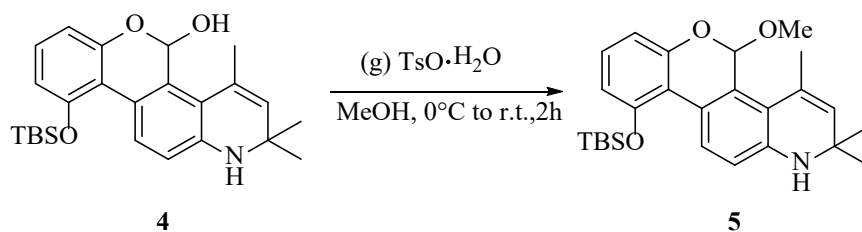
10-(tert-Butyldimethylsilyloxy)-5-oxo-2,5-dihydro-2,2,4-trimethyl-1H-[1]benzopyrano[3,4-f]quinoline (3). The solution of Phenol **2** (4.40 g, 14.4 mmol) in dry THF (200 mL) was cooled to 0 °C. Then the Imidazole (2.93 g, 43.2 mmol) and TBSCl (3.26 g, 21.6 mmol) were added. The

resulting mixture was stirred overnight at r.t. The reaction mixture was diluted with EtOAc (200 mL) and washed with 1 N HCl (3 × 50 mL), saturated NaHCO₃ (2 × 50 mL) and brine (3 × 50 mL). The organic layer was dried (Na₂SO₄) and concentrated. The resulting residue was purified by chromatography on silica gel with 0 to 15% EtOAc in hexanes to give the desired compound **3** (3.51 g, 8.35 mmol, 58%) as a light yellow solid. ¹H NMR (400 MHz, DMSO) δ 8.64 (d, *J* = 8.9 Hz, 1H), 7.25 (t, *J* = 8.2 Hz, 1H), 7.07 (d, *J* = 9.0 Hz, 1H), 6.94 (dd, *J* = 8.2, 0.9 Hz, 1H), 6.86 (br, s, 1H), 6.83 (dd, *J* = 8.1, 1.0 Hz, 1H), 5.44 (br, s, 1H), 1.94 (s, 3H), 1.22 (s, 6H), 1.00 (s, 9H), 0.32 (s, 6H). HR-MS: Calculated for C₂₅H₃₂NO₃Si 422.2146 (M+H)⁺ determined 422.2141.



10-(tert-butyltrimethylsilyloxy)-5-hydroxy-2,5-dihydro-2,2,4-trimethyl-1H-

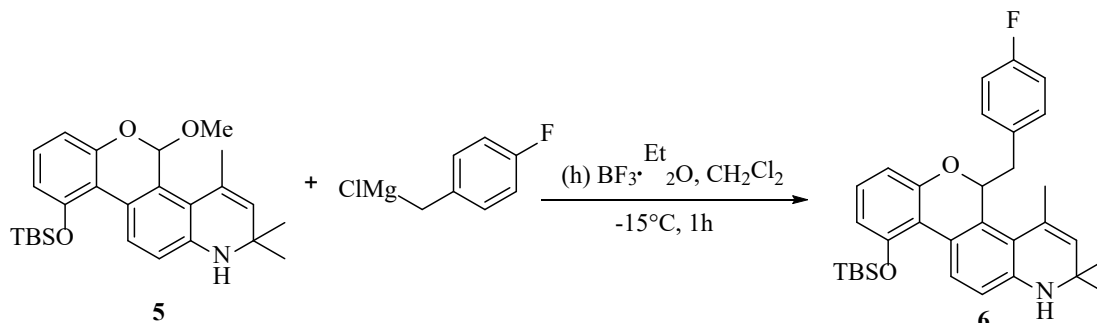
[1]benzopyrano[3,4-f]quinolone(4). Hemiactal lactol **3** (3.51 g, 8.35 mmol) in dry CH₂Cl₂(100 mL) was slowly added 1M Dibal-H in hexane (20.9 mL, 20.9 mmol) at -78 °C under Ar to form the orange-red solution and was stirred at -78 °C for 2 h. Then was quenched with 200 mL EtOAc and 200 mL of saturated aqueous Rochelle's salt, and mixture was stirred vigorously for 4 h at r.t. The separated aqueous layer was extracted with EtOAc, the combined organic layers were washed with brine, dried (Na₂SO₄) and concentrated to give the lactol **4** (2.83 g, 6.68 mmol, 80%) as a light yellow solid. ¹H NMR (400 MHz, DMSO) δ 7.99 (d, *J* = 8.6 Hz, 1H), 6.98 (t, *J* = 8.1 Hz, 1H), 6.92 (d, *J* = 4.9 Hz, 1H), 6.69 – 6.47 (m, 4H), 6.08 (br, 1H), 5.41 (br, 1H), 2.23 (s, 3H), 1.26 (s, 3H), 1.08 (s, 3H), 0.97 (s, 9H), 0.25 (s, 3H), 0.10 (s, 3H). Calculated for C₂₅H₃₂NO₃Si 422.2157 (M-H)⁻ determined 422.2147.



10-(tert-butyltrimethylsilyloxy)-5-methoxy-2,5-dihydro-2,2,4-trimethyl-1H-

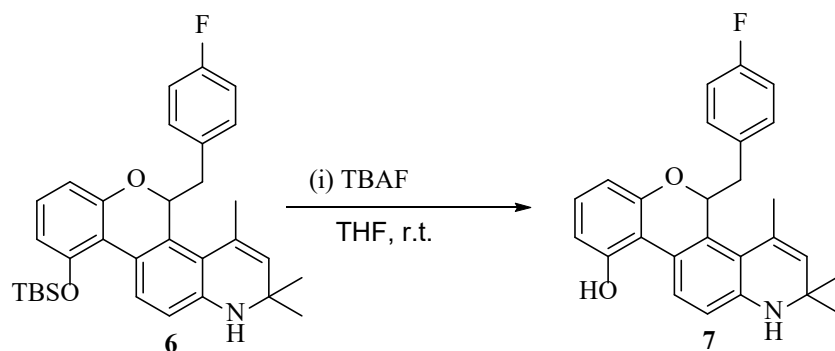
[1]benzopyrano[3,4-f]quinoline (5). The lactol **4** (2.83 g, 6.68 mmol) was dissolved in 60 mL of MeOH at 0 °C, treated with the solution of *p*-TsOH·H₂O (550 mg) in MeOH and stirred for 30 min at 0 °C. Then the cool bath was removed and stirred at r.t. for 1 h. The reaction mixture was concentrated under reduced pressure to remove most of MeOH. Then the EtOAc(200 mL) was added and the organic layers were washed with saturated aqueous NaHCO₃, brine, dried (Na₂SO₄),

and concentrated. The resulting brown oil was purified by flash chromatography using silica gel with 0 to 12% EtOAc in hexane to give the desired compound **5** (2.27 g, 5.21 mmol, 78%) as an off-white powder. ¹H NMR (400 MHz, DMSO) δ 7.94 (d, *J* = 8.5 Hz, 1H), 6.97 (t, *J* = 8.0 Hz, 1H), 6.66 (d, *J* = 7.8 Hz, 1H), 6.57 (m, 2H), 6.13 (m, 2H), 5.39 (br, 1H), 3.29 (s, 3H), 2.13 (s, 3H), 1.22 (s, 3H), 1.03 (s, 3H), 0.91 (s, 9H), 0.19 (s, 3H), 0.04 (s, 3H). Calculated for C₂₆H₃₆NO₃Si 438.2459 (M+H)⁺ determined 438.2456.

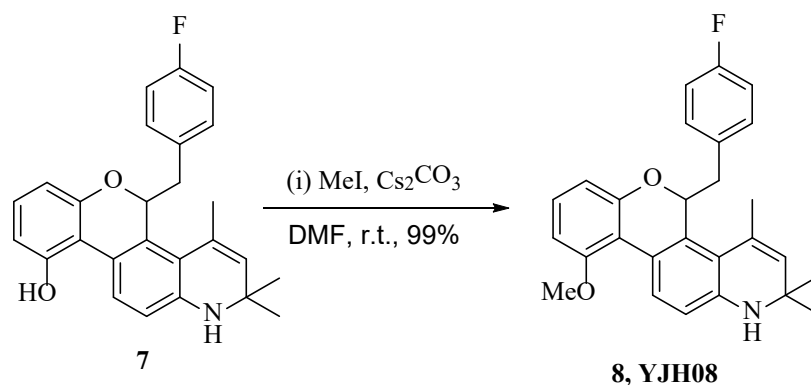


10-(tert-Butyldimethylsilyloxy)-5-(4-fluorobenzyl)-2,5-dihydro-2,2,4-trimethyl-1H-

[1]benzopyrano[3,4-f]quinoline (6). To the solution of **5** (437 mg, 1.00 mmol) in 10 mL dry CH₂Cl₂ was cooled to -15 °C and treated with BF₃·Et₂O (370 μL, 3.00 mmol) dropwise via syringe. The resulting deep green solution was stirred for 30 min at -15 °C, treated dropwise with 4-fluorobenzylmagnesium chloride (36.0 mL of a 0.25 M in THF solution, 9.00 mmol). At the end of the addition, the green color dissipated to give a slightly yellow solution. After the solution was stirred for 15 min at -15 °C, the reaction mixture was quenched by the addition of 20 mL of saturated aqueous NaHCO₃ followed by 100 mL of EtOAc and the layers separated. The aqueous phase was extracted with EtOAc, and the combined organic phases were washed with brine and dried over Na₂SO₄. The residue was purified by silica gel chromatography to give the desired compound **6** (268 mg, 0.52 mmol, 52%) as an off-white powder. ¹H NMR (400 MHz, DMSO) δ 7.97 (d, *J* = 8.6 Hz, 1H), 7.09 (d, *J* = 7.3 Hz, 4H), 7.03 (t, *J* = 8.1 Hz, 1H), 6.60 (d, *J* = 8.6 Hz, 2H), 6.48 (d, *J* = 7.9 Hz, 1H), 6.11 (br, 1H), 5.91 (dd, *J* = 9.7, 3.6 Hz, 1H), 5.39 (br, 1H), 2.97 (m, 1H), 2.84 (m, 1H), 2.20 (s, 3H), 1.14 (s, 6H), 0.94 (s, 9H), 0.22 (s, 3H), 0.11 (s, 3H). ¹³C NMR (100 MHz, DMSO-d₆) δ 151.86 (d, *J* = 50.3 Hz), 146.08, 134.42, 134.38, 133.72, 132.16, 131.26, 131.18, 127.90, 127.74, 127.27, 117.11, 116.85, 116.67, 115.40 (d, *J* = 21.0 Hz), 114.97, 113.53, 111.52, 75.17, 50.19, 37.44, 29.70, 29.46, 26.30, 24.69, 18.64. Calculated for C₃₂H₃₉FNO₂Si 516.2729 (M+H)⁺ determined 516.2735.

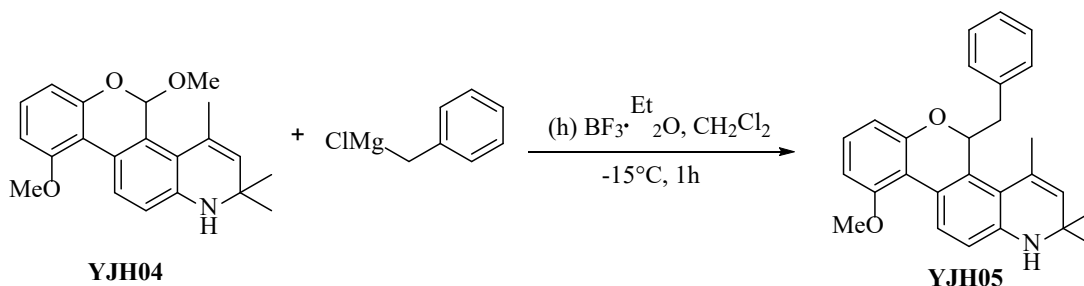


10-Hydroxy-5-(4-fluorobenzyl)-2,5-dihydro-2,2,4-trimethyl-1H-[1]benzopyrano[3,4-f]quinoline (7). Silyl ether **6** (1.39 g, 2.71 mmol) was dissolved in THF (20 mL) at r.t. and was treated with TBAF (5.42 mL of a 1 M solution in THF, 5.42 mmol). After 2 h, the reaction mixture was concentrated in vacuo and was redissolved in EtOAc (60 mL). The solution was washed with brine (10 mL), then was dried (Na_2SO_4). The residue was purified by silica gel chromatography to give the desired phenol **7** (739 mg, 1.84 mmol, 68%) as an off-white powder. ^1H NMR (400 MHz, DMSO) δ 9.86 (br, 1H), 8.20 (d, $J = 8.6$ Hz, 1H), 7.19 – 7.05 (m, 4H), 6.94 (t, $J = 8.0$ Hz, 1H), 6.62 (dd, $J = 13.1, 8.4$ Hz, 2H), 6.31 (d, $J = 7.8$ Hz, 1H), 6.04 (br, 1H), 5.91 (d, $J = 7.5$ Hz, 1H), 5.40 (br, 1H), 3.00 (m, 1H), 2.73 (m, 1H), 2.21 (s, 3H), 1.16 (s, 3H), 1.13 (s, 3H). ^{13}C NMR (100 MHz, DMSO- d_6) δ 161.33 (d, $J = 241.9$ Hz), 154.76, 151.42, 145.73, 134.63 (d, $J = 3.0$ Hz), 133.93, 131.73, 131.25 (d, $J = 8.0$ Hz), 127.90, 127.50, 127.28, 117.33, 116.77, 115.33 (d, $J = 21.0$ Hz), 113.79, 112.38, 110.33, 108.96, 74.93, 50.11, 37.79, 29.45, 24.75. ^{19}F NMR (376 MHz, DMSO- d_6) δ -116.94. Calculated for $\text{C}_{26}\text{H}_{25}\text{FNO}_2$ 402.1864 ($\text{M}+\text{H}$) $^+$ determined 402.1861.



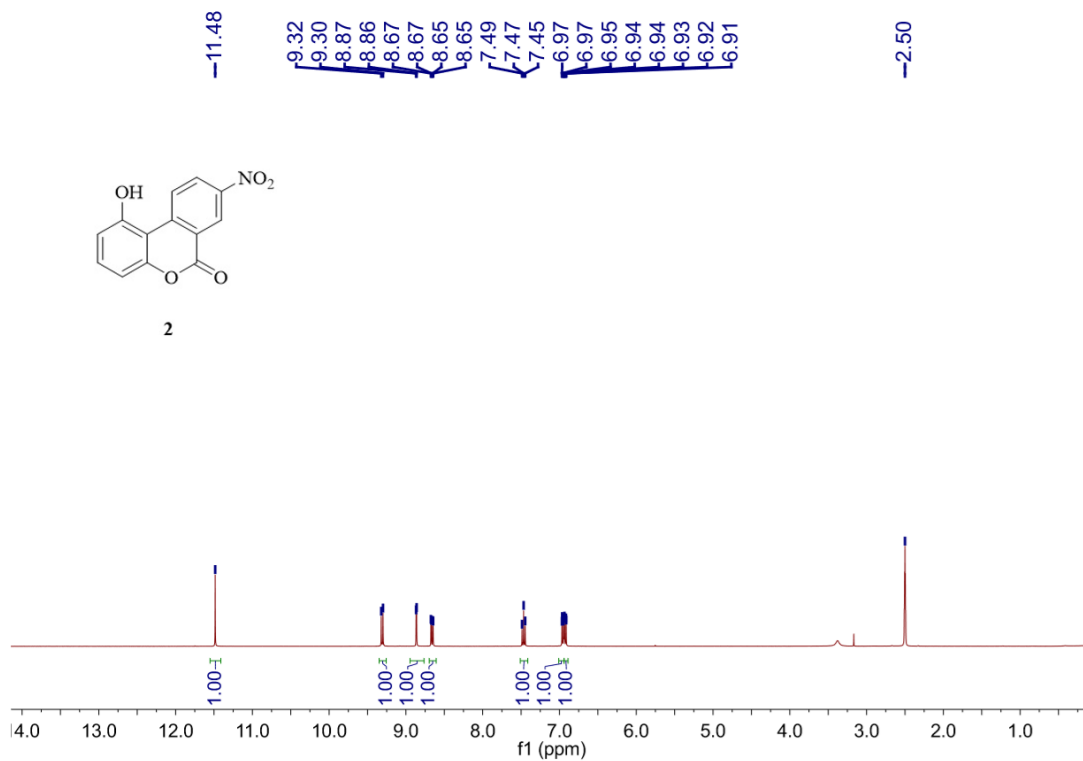
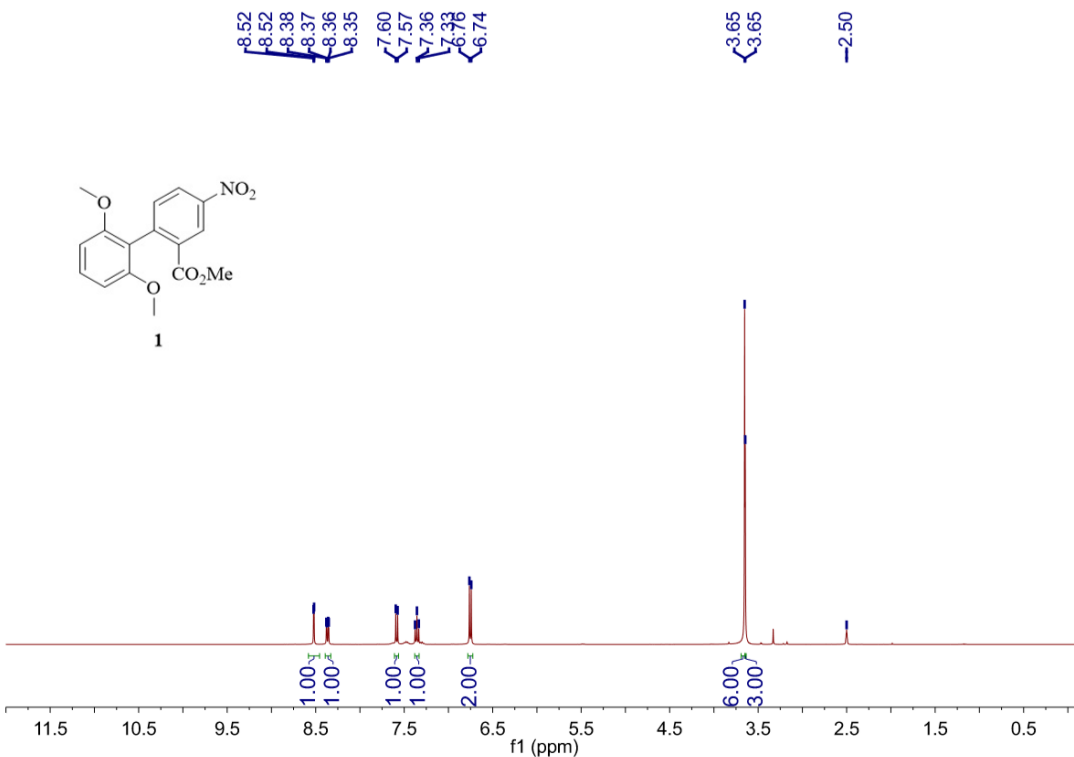
5-(4-fluorobenzyl)-10-methoxy-2,2,4-trimethyl-2,5-dihydro-1H-chromeno[3,4-f]quinoline(8). A dry, two-necked 100 mL round bottom flask equipped with a mechanical stirrer was charged with **7** (401 mg, 1 mmol) and anhydrous cesium carbonate (650 mg, 2 mol) in DMF (15 mL). Methyl iodide (564 mg, 4 mol) was then added in a dropwise fashion via syringe. After 4 h, the reaction was quenched by addition of H_2O (30 mL). A solution of 50% EtOAc/hexanes (50 mL) was added, and the mixture was stirred 15 min. The mixture was filtered, washed with

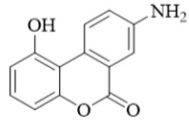
water (100 mL) and dried under vacuum to afford **8** (410 mg, 0.99 mmol, 99%) as a light yellow solid. ^1H NMR (400 MHz, DMSO- d_6) δ 8.01 (d, J = 8.6 Hz, 1H), 7.13 – 7.07 (m, 5H), 6.74 (d, J = 7.8 Hz, 1H), 6.62 (d, J = 8.6 Hz, 1H), 6.46 (d, J = 8.0 Hz, 1H), 6.15 (s, 1H), 5.96 – 5.88 (m, 1H), 5.41 (s, 1H), 3.88 (s, 3H), 2.96 (dd, J = 14.8, 10.1 Hz, 1H), 2.75 (dd, J = 14.8, 3.2 Hz, 1H), 2.21 (s, 3H), 1.15 (s, 3H), 1.12 (s, 3H). ^{13}C NMR (100 MHz, DMSO- d_6) δ 161.35 (d, J = 241.8 Hz), 158.66, 156.73, 151.16, 146.07, 134.48 (d, J = 3.0 Hz), 133.98, 132.04, 131.22 (d, J = 8.0 Hz), 127.83, 127.60, 119.28, 116.79, 116.52, 115.35 (d, J = 21.0 Hz), 113.85, 110.89, 105.96, 74.96, 56.12, 50.13, 37.60, 29.46, 24.74. ^{19}F NMR (376 MHz, DMSO- d_6) δ -116.88 (m, 1F). Calculated for $\text{C}_{27}\text{H}_{26}\text{O}_2\text{NF}$: 415.1942 (M) $^+$ determined 415.1939.



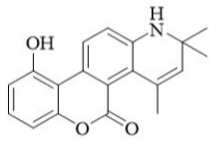
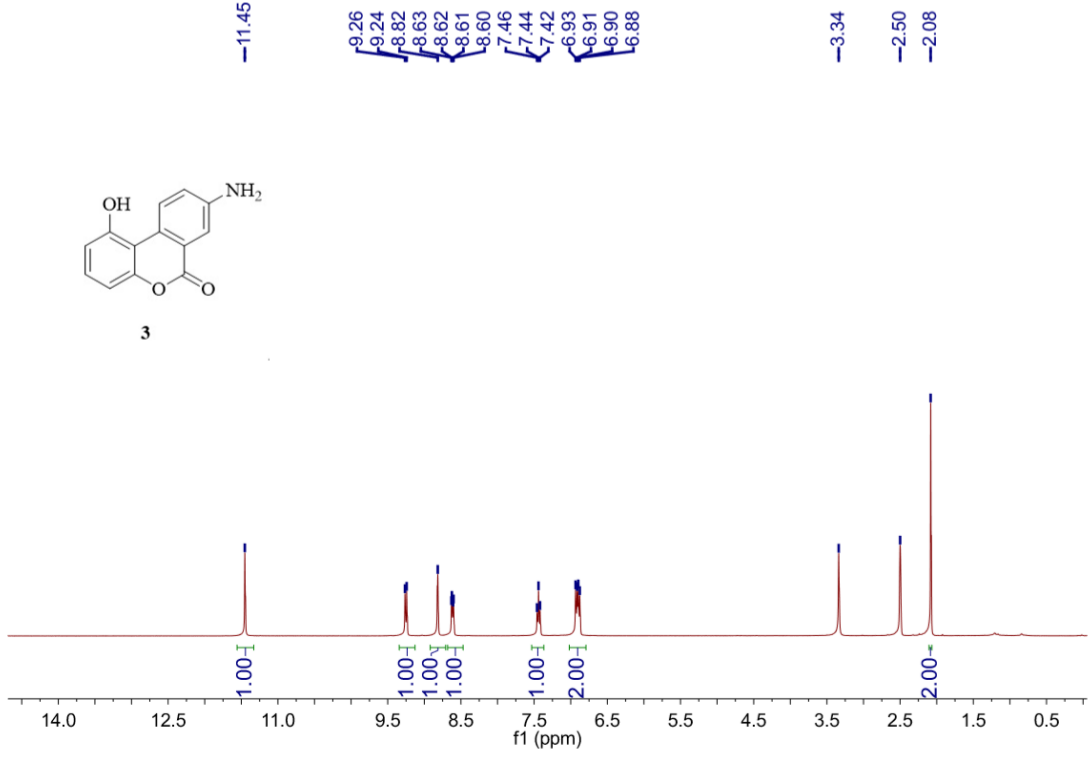
10-(tert-Butyldimethylsiloxy)-5-benzyl-2,5-dihydro-2,2,4-trimethyl-1H-[1]benzopyrano[3,4-f]quinoline (YJH05). To the solution of **YJH04** (337 mg, 1.00 mmol) in 3 mL dry CH_2Cl_2 was cooled to -15°C and treated with $\text{BF}_3 \cdot \text{Et}_2\text{O}$ (370 μL , 3.00 mmol) dropwise via syringe. The resulting deep green solution was stirred for 30 min at -15°C , treated dropwise with benzylmagnesium chloride (36.0 mL of a 0.25 M in THF solution, 9.00 mmol). At the end of the addition, the green color dissipated to give a slightly yellow solution. After the solution was stirred for 15 min at -15°C , the reaction mixture was quenched by the addition of 20 mL of saturated aqueous NaHCO_3 followed by 100 mL of EtOAc and the layers separated. The aqueous phase was extracted with EtOAc , and the combined organic phases were washed with brine and dried over Na_2SO_4 . The residue was purified by silica gel chromatography to give the desired compound **YJH05** (269 mg, 0.68 mmol, 68%) as an off-white powder. ^1H NMR (400 MHz, DMSO) δ 8.01 (d, J = 8.9, 1H), 7.30 – 7.17 (m, 3H), 7.10 (m, 3H), 6.73 (d, J = 7.8 Hz, 1H), 6.64 (d, J = 8.8 Hz, 1H), 6.45 (d, J = 7.9 Hz, 1H), 6.12 (d, J = 2 Hz, 1H), 5.90 (dd, J = 2.9, 9.8 Hz, 1H), 5.41 (s, 1H), 3.89 (s, 3H), 2.97 (dd, J = 9.8, 14.9 Hz, 1H), 2.72 (dd, J = 2.8, 14.8 Hz, 1H), 2.22 (s, 3H), 1.16 (s, 3H) 1.15 (s, 3H). LCMS: m/z (M+H) $^+$ 398.

Copies of NMR spectrum

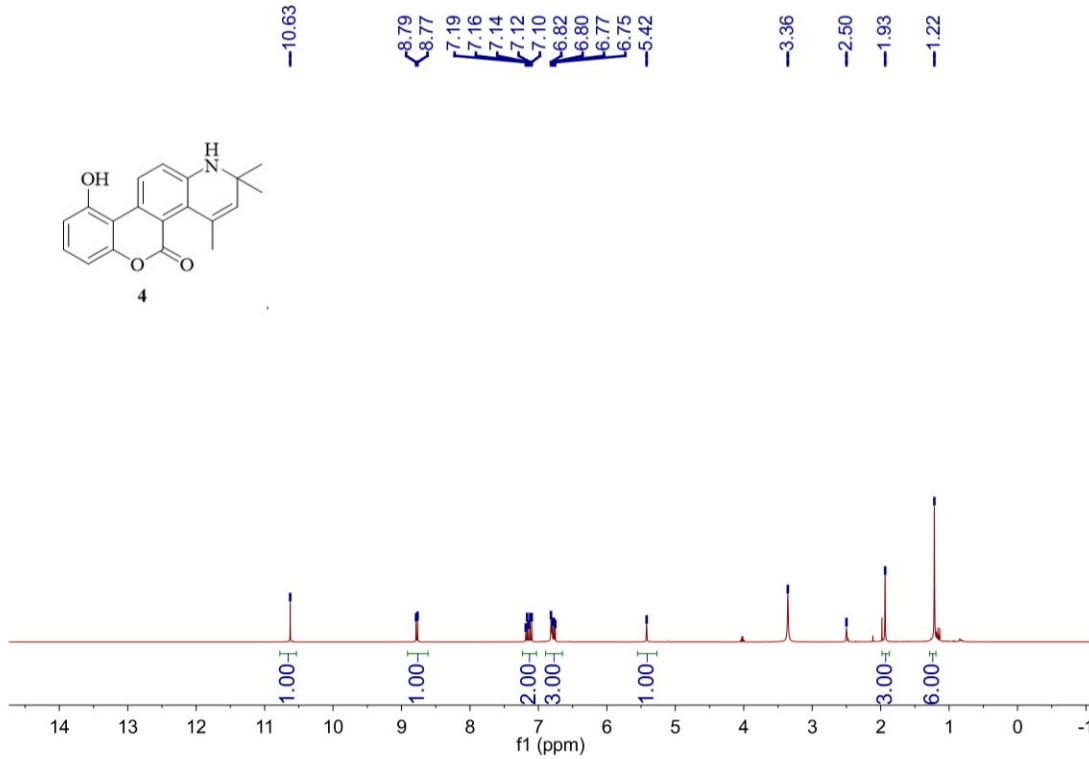


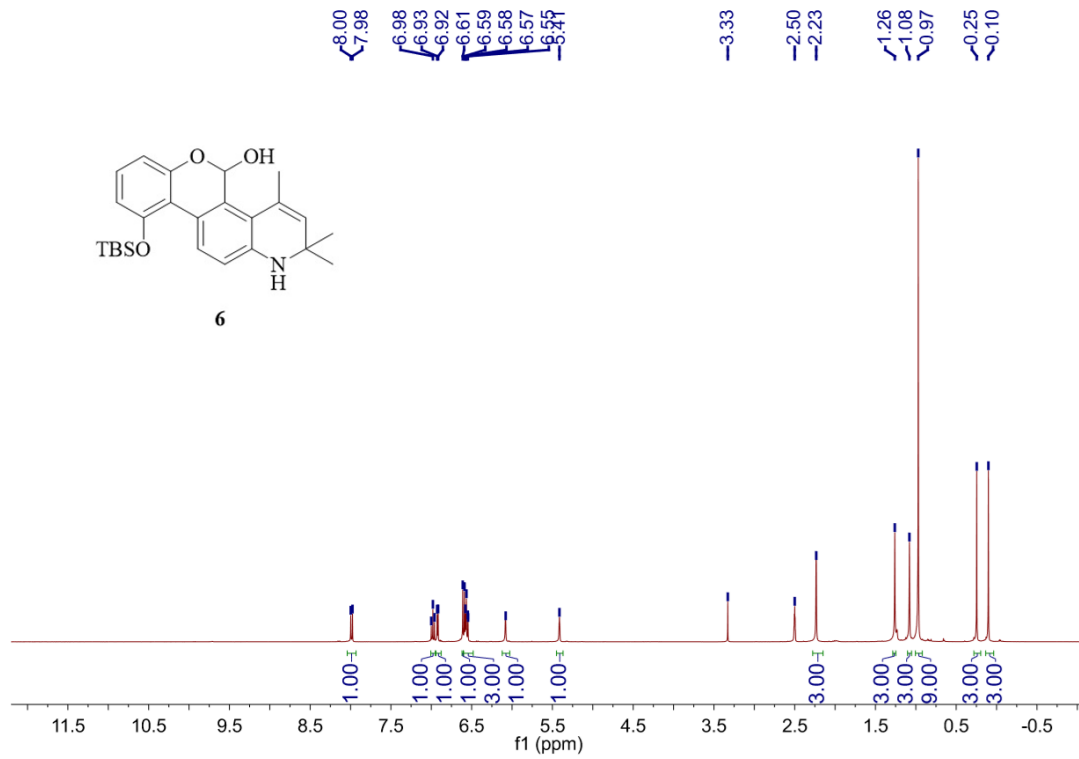
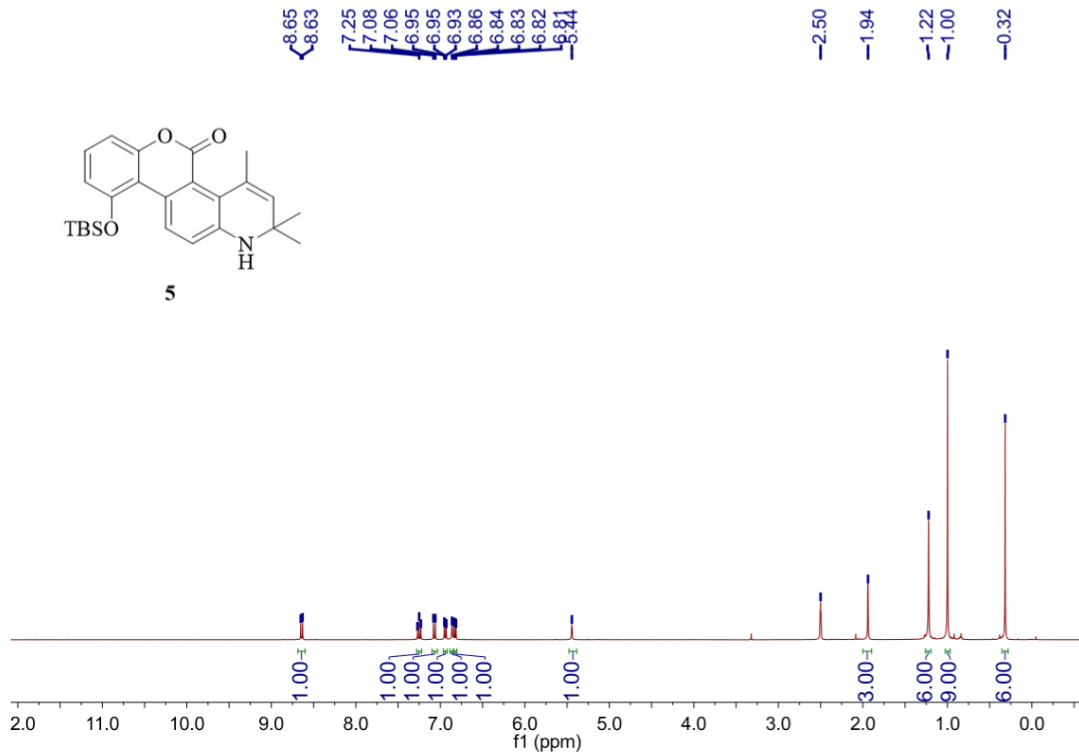


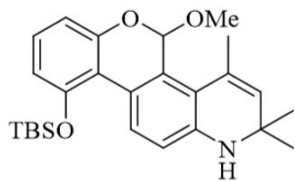
3



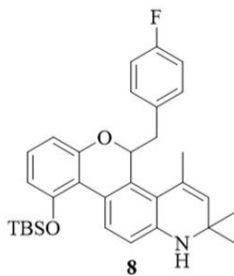
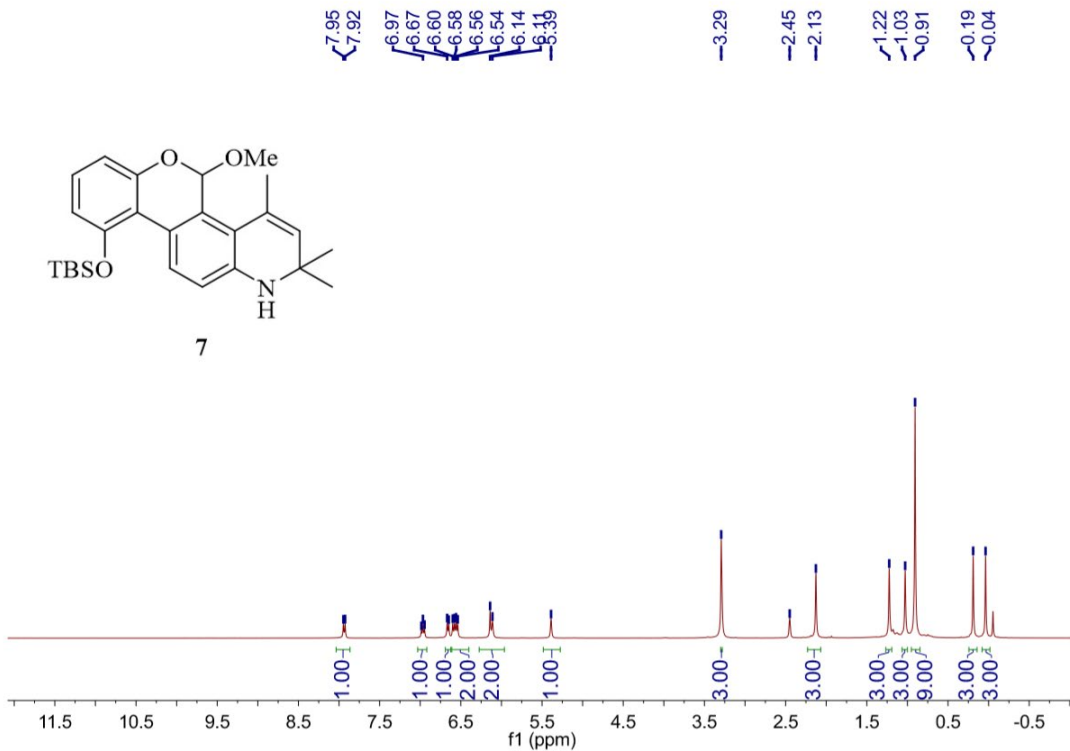
4



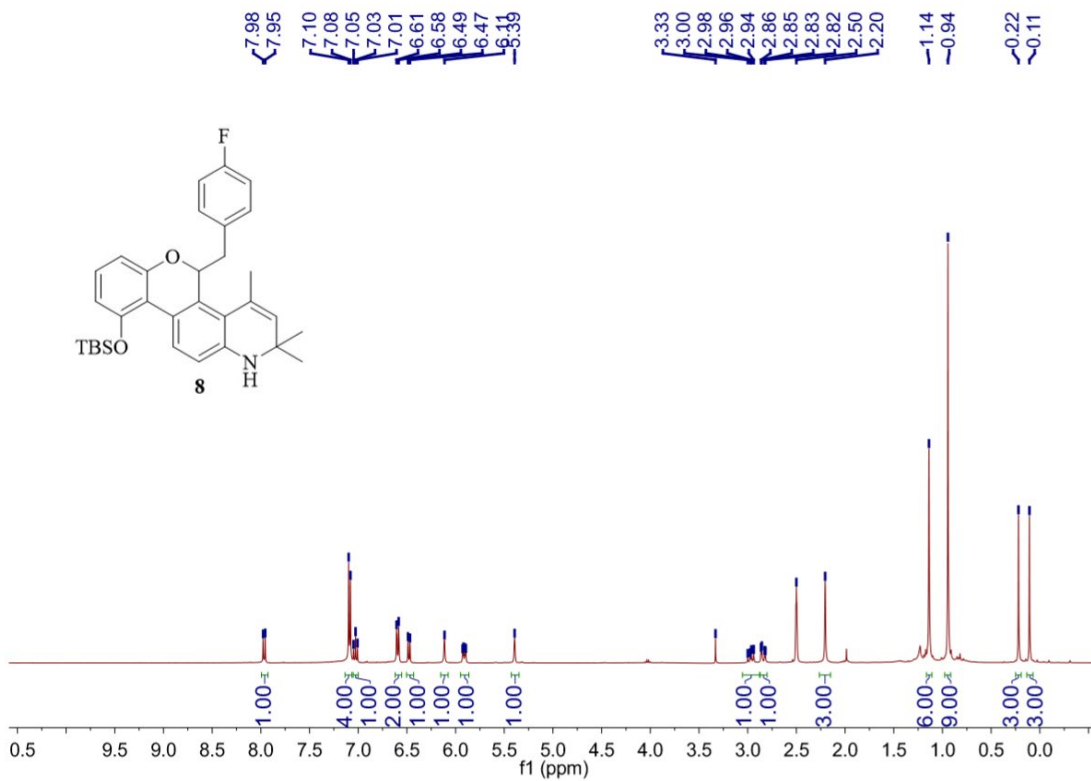


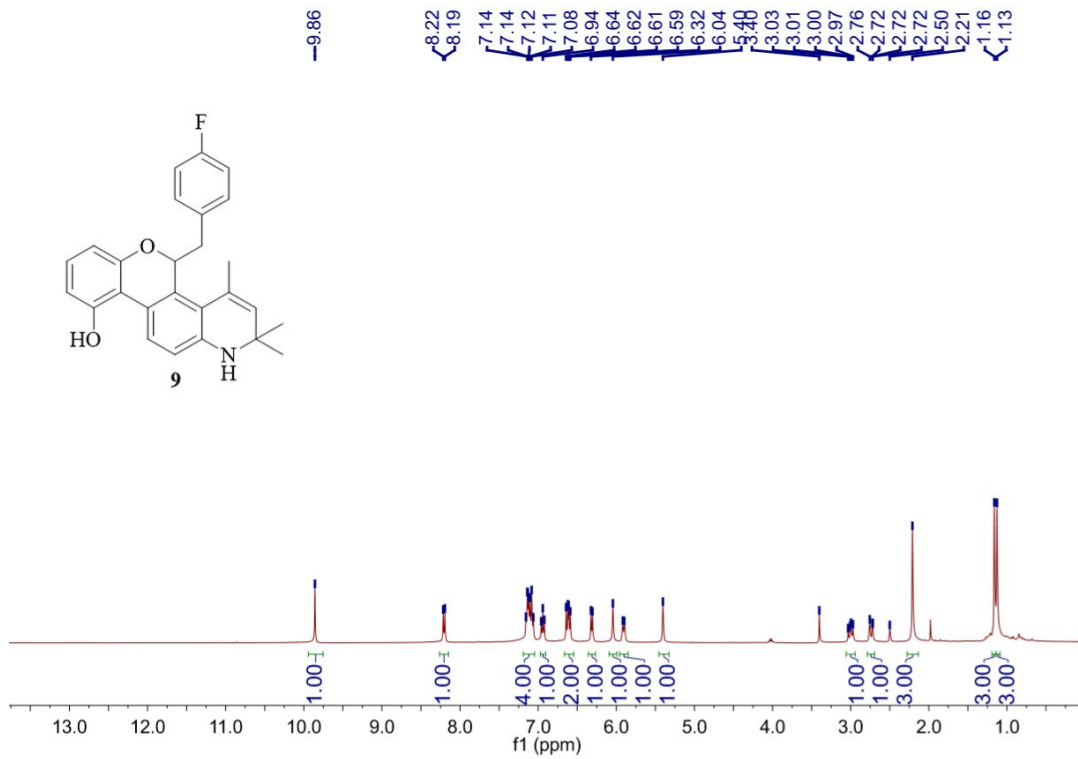
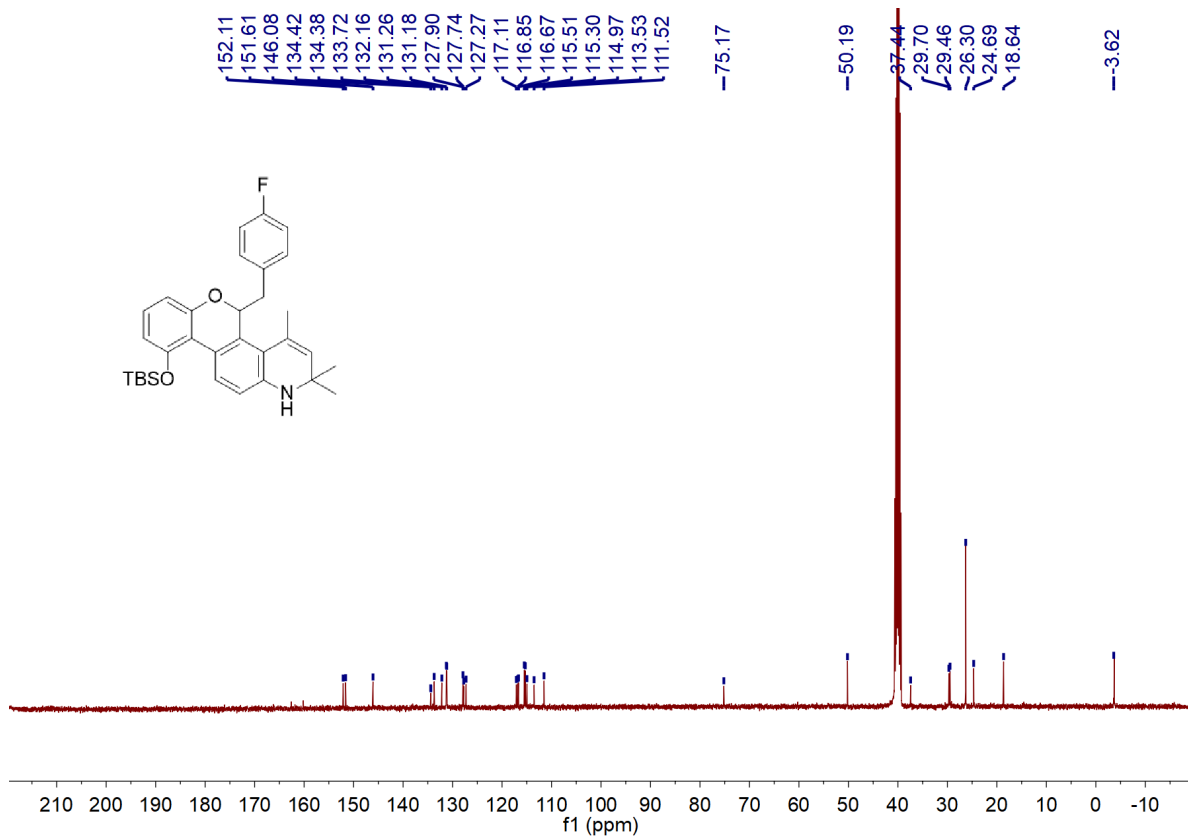


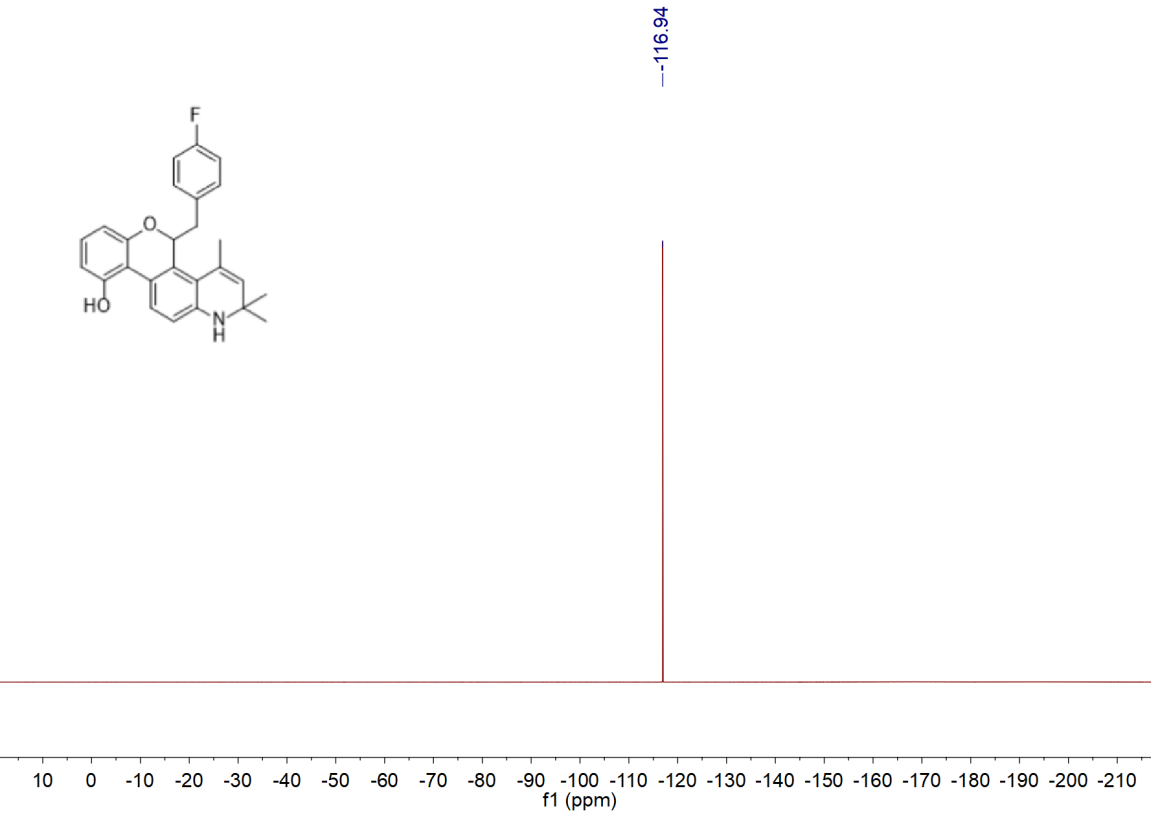
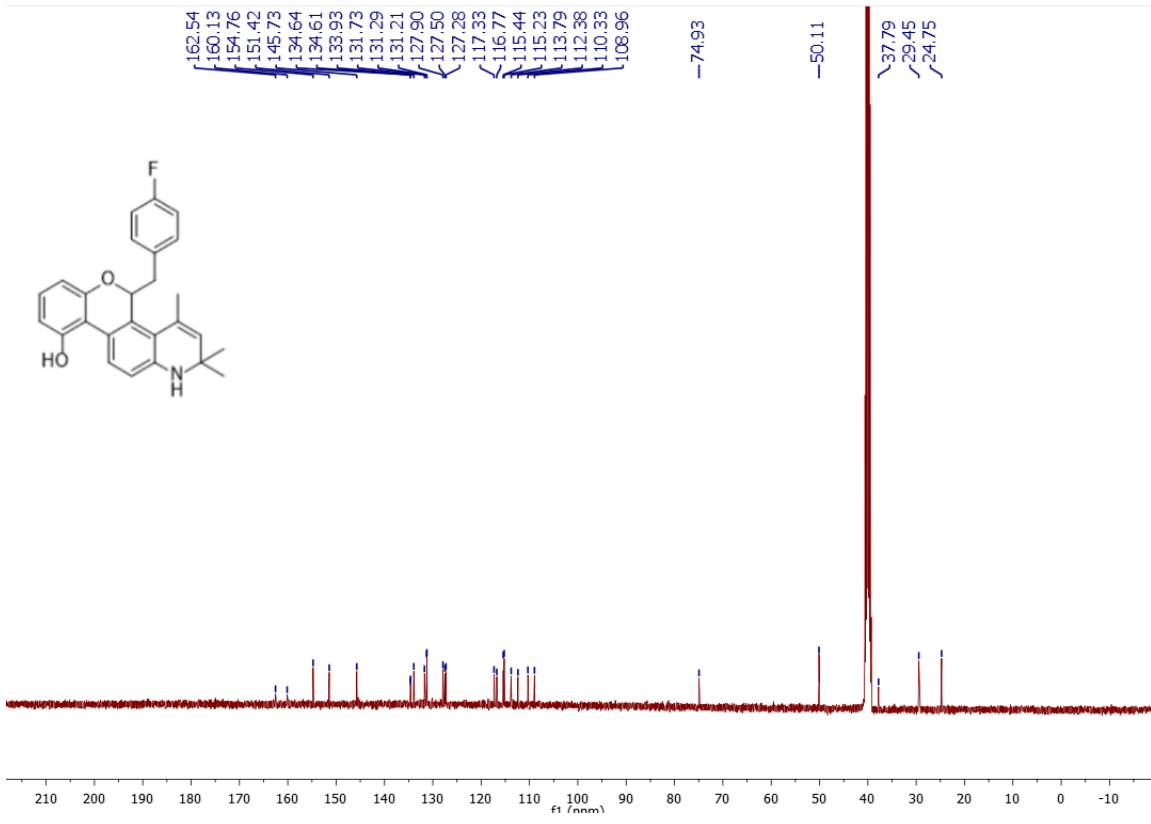
7

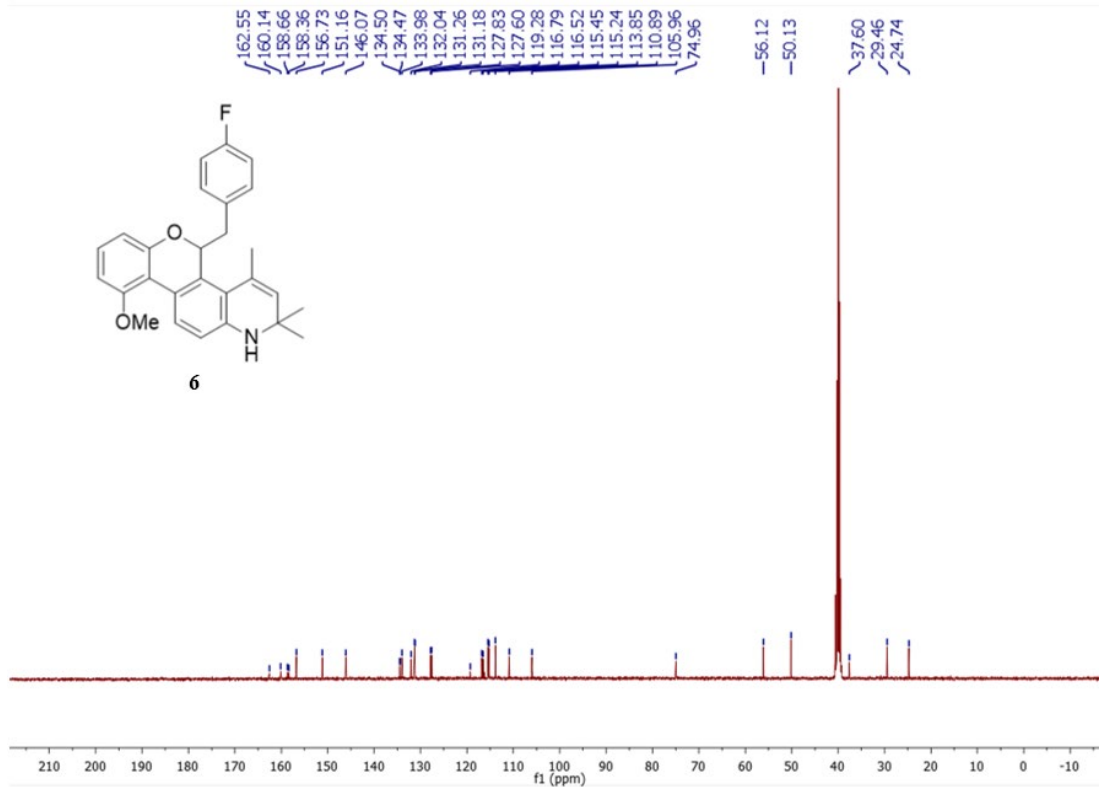
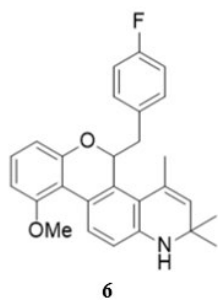
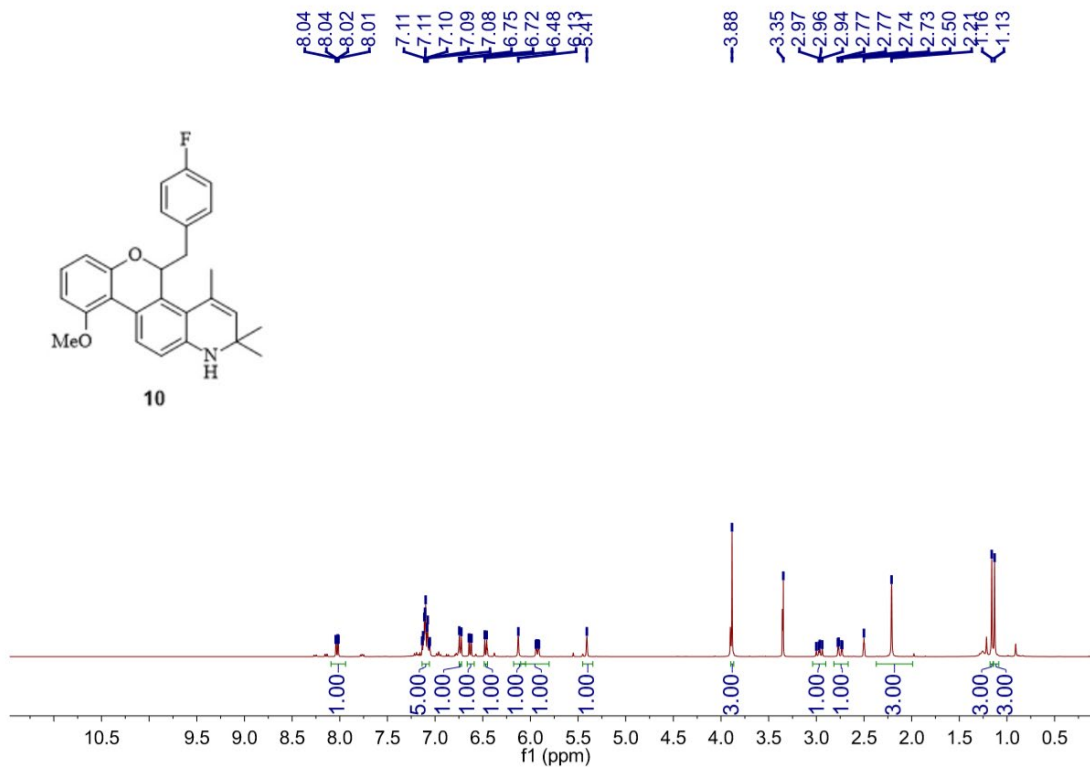
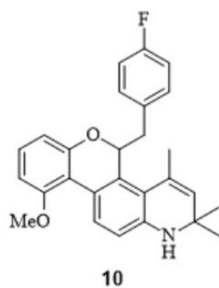


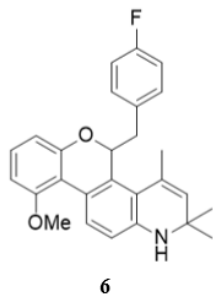
8











-116.84
-116.85
-116.86
-116.88
-116.90
-116.92

